



**Faculty of Science and Technology**

## **MASTER'S THESIS**

Study program/ Specialization: Master in Environmental Technology / Offshore Environmental Engineering	Spring semester, 2011  Open / <del>Restricted</del> access
Writer: Dian Ekawati	..... (Writer's signature)
Faculty supervisor: Tor Hemmingsen External supervisor(s):	
Title of thesis:  Effect of Temperature, Bicarbonate, and MEG Concentration on Pre-corroded Carbon Steels	
Credits (ECTS): 30	
Key words: CO <sub>2</sub> corrosion pH stabilization iron carbonate X-65 St-52 MEG	Pages: 82  + enclosure: 11  Stavanger, June, 14 <sup>th</sup> , 2011 Date/year

**Effect of Temperature, Bicarbonate, and MEG  
Concentration on Pre-corroded Carbon Steels**

**Dian Ekawati**

*June, 14<sup>th</sup>, 2011*

**University of Stavanger**

## ABSTRACT

CO<sub>2</sub> corrosion in carbon steel has been a major problem in many of oil and gas fields for years. One method that has been known to be effective for corrosion control especially in pipeline is pH stabilization. This method is often combined with MEG injection for hydrate prevention. pH stabilization utilizes chemical, mostly bases for adjusting pH to an optimum value that encourages protective FeCO<sub>3</sub> formation. This master thesis project is aimed to find the effect of MEG concentration, bicarbonate, temperature, and steel type on CO<sub>2</sub> corrosion of pre-corroded steel. The addition of MEG ranged between 0-50% wt, while bicarbonate concentration was between 0-100 mmol/kg. Experiments were performed on pre-corroded X-65 and St-52 steel by applying anodic current of 0.25 mA/cm<sup>2</sup> for 24 hours, at temperature 20°C and 40°C. Effect of those parameters on the corrosion reactions was characterized by iron concentration, Rp/Ec trend, and potentiodynamic polarization measurements.

The results from the experiments showed a decrease in corrosion rate with the increase in MEG and HCO<sub>3</sub><sup>-</sup> concentration. These effects were observed in Rp/Ec trend and potentiodynamic sweep. Temperature on the other hand increased the corrosion rate, except under conditions where protective iron carbonate film was most likely formed. Some indication of FeCO<sub>3</sub> formation and steel passivation were detected in 100 mmol/kg HCO<sub>3</sub><sup>-</sup>, 50% MEG, and 40°C in both steels. Only at this condition pitting was observed, while the other conditions showed uniform corrosion. The corrosion rate was found to be higher than 1 mm/y in case of uniform corrosion, in which St-52 attained higher corrosion rate compared to X-65 due to higher carbon content. Under formation of protective FeCO<sub>3</sub> film, the corrosion rate decreased to 0.34 and 0.24 mm/y for X-65 and St-52 respectively.

## **ACKNOWLEDGMENT**

This thesis is prepared as a requirement to fulfil Msc degree in Faculty of Science and Technology at the University of Stavanger. I would like to express gratitude and appreciation to my supervisor, Prof. Tor Hemmingsen for his dedication, direction, and supervision on this project. This thesis would not have been possible to be completed without his patience, guidance and valuable advices throughout many extensive discussions. Constructive ideas from Tonje Berntsen and Marion Seiersten from IFE are very helpful and I thank them for the enlightenment. I want to acknowledge Liv Margareth Aksland, and Jan Kare Bording for their support during my lab works. I would thank University of Stavanger for awarding me the scholarship to continue studying in the university.

I also want to thank all of my colleagues, friends, and family in Indonesia for their love, support and encouragement so that I can accomplish my master degree. Above all, I am grateful to Allah for such an opportunity in my life.

## TABLE OF CONTENTS

ABSTRACT .....	2
ACKNOWLEDGMENT .....	3
LIST OF FIGURE .....	6
LIST OF TABLE .....	8
1. INTRODUCTION .....	9
2. THEORY.....	11
2.1 CO <sub>2</sub> Corrosion.....	11
2.1.1 <i>Cathodic Reactions</i> .....	11
2.1.2 <i>Anodic Reactions</i> .....	12
2.1.3 <i>Corrosion Damage</i> .....	14
2.1.4 <i>Factor Affecting CO<sub>2</sub> Corrosion</i> .....	14
2.2 Corrosion Film Formation.....	18
2.2.1 <i>Transparent Film</i> .....	19
2.2.2 <i>Iron Carbide Film (Fe<sub>3</sub>C)</i> .....	19
2.2.3 <i>Iron Carbonate Film</i> .....	22
2.2.4 <i>Iron Carbonate plus Iron Carbide Film</i> .....	24
2.3 Corrosion Control using pH Stabilization Method .....	27
3. EXPERIMENTAL METHOD .....	31
3.1 Test Specimen and Solution Preparation.....	32
3.2 Equipment Set Up .....	34
3.3 Potentiostat .....	35
3.4 Corrosion Rate Calculation.....	36

3.5	Electrochemical Test Result Validation .....	37
3.5.1	<i>Iron Content Analysis</i> .....	37
3.5.2	<i>Weight Loss Measurement</i> .....	38
3.6	Surface Analysis using Scanning Electron Microscopy.....	39
4.	RESULT AND DISCUSSION.....	40
4.1	Corrosion Potential.....	40
4.2	Galvanostatic Measurement.....	45
4.3	Rp/Ec Trend.....	51
4.3.1	<i>Corrosion Current</i> .....	51
4.3.2	<i>Corrosion Potential</i> .....	58
4.4	Iron Concentration Analysis .....	62
4.5	Potentiodynamic Scans.....	68
4.6	Future Works and Recommendation.....	75
5.	CONCLUSION .....	76
6.	REFERENCES .....	78
	APPENDIX A – STEEL CERTIFICATE.....	83
	APPENDIX B - STANDARD CALIBRATION CURVE.....	85
	APPENDIX C – CATHODIC POTENTIODYNAMIC SWEEP .....	86
	APPENDIX D – WEIGHT LOSS .....	90
	APPENDIX E - SEM IMAGES AND EDS ANALYSIS.....	91

## LIST OF FIGURE

Figure 1. Schematic drawing of carbide (cementite) lamellas and the surrounding corroding ferritic-pearlitic steel (left is freshly ground surface, and right is corroded surface) .....	21
Figure 2. Different morphologies observed for protective and nonprotective corrosion layer .....	25
Figure 3. Sample mounted in working electrode holder .....	33
Figure 4. Equipment set up .....	35
Figure 5. Corrosion potential of series 0-100 mmol/kg $\text{HCO}_3^-$ , at 20°C .....	41
Figure 6. Cathodic potentiodynamic sweep of (a) X-65 and (b) St-52 in 50% MEG, 0-100 mmol/kg $\text{HCO}_3^-$ , at 20°C .....	42
Figure 7. Corrosion potential of series 0-100 mmol/kg $\text{HCO}_3^-$ , at 40°C .....	44
Figure 8. Potential under 0.25 mA/cm <sup>2</sup> applied current of series 0-100 mmol/kg $\text{HCO}_3^-$ , at 20°C.....	46
Figure 9. Potential due to 0.25 mA/cm <sup>2</sup> applied current of series 0-100 mmol/kg $\text{HCO}_3^-$ , at 40°C.....	49
Figure 10. Potentials at 0.25 mA/cm <sup>2</sup> applied current on Pt electrode, with 1 bar CO <sub>2</sub> purged, 1% wt NaCl, 40°C, and 20-60% MEG addition.....	51
Figure 11. Corrosion current measurement on series 0-100 mmol/kg $\text{HCO}_3^-$ at 20°C.....	53
Figure 12. Corrosion current measurement on series 0-100 mmol/kg $\text{HCO}_3^-$ , at 40°C.....	55

Figure 13. Corrosion potential measurement on series 0-100 mmol/kg $\text{HCO}_3^-$ , at 20°C.....	59
Figure 14. Corrosion potential measurement on series 0-100 mmol/kg $\text{HCO}_3^-$ , at 40°C.....	60
Figure 15. Potentiodynamic sweep on series 0-100 mmol/kg $\text{HCO}_3^-$ , at 20°C....	70
Figure 16. Potentiodynamic sweep on series 0-100 mmol/kg $\text{HCO}_3^-$ , at 40°C....	71
Figure 17. Sample surface after experiment (a. Series 100 mmol/kg $\text{HCO}_3^-$ , 50% MEG at 40°C; b. Series 0 mmol/kg $\text{HCO}_3^-$ , 0% MEG at 20°C).....	74
Figure 18. SEM images of the X-65 electrodes applied with the anodic current density of 1 mA/cm <sup>2</sup> for 24 hours.....	75

## LIST OF TABLE

Table 1. Overview of some fields where pH stabilization has been applied .....	30
Table 2. Experimental matrix .....	31
Table 3. Elemental analysis (%wt) of steel specimen (from certificate) .....	32
Table 4. Electrochemical test parameter .....	36
Table 5. Chemical reactions and the equilibrium constant .....	63
Table 6. Formula to calculate equilibrium constant for reactions in Table 5.....	64
Table 7. Estimated iron concentration required for saturation.....	64
Table 8. Iron analysis result .....	66

## 1. INTRODUCTION

High energy demand and limited available hydrocarbon reservoir that has been found are now pushing the industry toward searching for new sources. Current technology permits exploration and production of oil and gas from deeper sea, and harsher environment. This in turn will give new challenges in the corrosion aspect of transportation and processing facilities. Beside extreme weather, exploitation of reservoir with high acid gas and other impurities content make the corrosion problem more complicated. Most common acid gases found with hydrocarbon production are CO<sub>2</sub> and H<sub>2</sub>S.

Oil and gas processing is commonly carried out in onshore or offshore central processing facilities due to safety and economic consideration. The hydrocarbon is produced together with produced water and all impurities from wellhead, and then transported further to processing plant. A number of long pipelines have been constructed under the sea surface stretching hundreds of kilometres from the producing wells to the plant, such as Troll and Huldra. Thus it is required to have a reliable pipeline for fluid transportation. Carbon steel is often selected as base material because of its mechanical characteristic and economic feasibility. However, this material has limitation, especially in corrosion resistance which is inferior compared to other material such as stainless steel or duplex.

In gas producing fields, hydrate formation is prevented by injecting glycol near the wellhead. Hydrate is a solid crystal which will be formed if there is condensed water in a hydrocarbon gas, at pressure and temperature below the hydrate formation point. Hydrate formation need to be avoided because it can plug pipelines that may cause operational problem and disturb production. In addition to its function as hydrate inhibitor, glycol is known to reduce the corrosion rate in the presence of CO<sub>2</sub>.

This thesis focuses mainly on sweet corrosion of different carbon steel qualities. CO<sub>2</sub> corrosion has been a problem for oil and gas industries for years. Many attempts have been made in characterization of CO<sub>2</sub> corrosion, and various

methods to overcome it. One of the methods which have been proven efficient and widely used today is pH stabilization. Currently, detailed mechanism of this method is still in further investigation. Deeper knowledge on how pH stabilization works, parameters that can affect the corrosion protection and characteristic on certain steel will be beneficial in optimizing field application.

In this thesis, pH stabilization method is emphasized. This study is aimed to find the effect of MEG concentration, bicarbonate, temperature, and steel type on CO<sub>2</sub> corrosion of pre-corroded carbon steel. Anodic galvanostatic by applying constant current over a period of time was performed as a pre-corrosion step. Effect of those parameters on the corrosion reactions will be characterized by iron concentration,  $R_p/E_c$  trend, and potentiodynamic polarization measurement.

## 2. THEORY

### 2.1 CO<sub>2</sub> Corrosion

CO<sub>2</sub> gas is soluble to hydrocarbon liquid and gas, as well as produced water. Corrosion problem for steel will arise if there is available aqueous phase that act as an electrolyte to promote the electrochemical reactions. Nordsveen et al. suggested that the presence of CO<sub>2</sub> in aqueous solution enhances corrosion rate in mild steel by increasing the rate of hydrogen evolution reaction. Detail of mechanism and chemical reactions occur during corrosion have been discussed in various studies [1-5].

#### 2.1.1 Cathodic Reactions

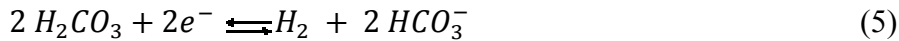
Initially, CO<sub>2</sub> will dissolve into water, where a fraction of it is hydrated and forms carbonic acid as written in Equations 1 and 2.



The carbonic acid is a weak acid, dissociates further in two steps producing bicarbonate and carbonate ions based on Equations 3 and 4.



The rate determining step for the whole process is believed to be CO<sub>2</sub> hydration (Equation 2) since the reaction progress slowly, and the hydration constant is small,  $2.58 \times 10^{-3}$  at 20°C [2]. H<sub>2</sub>CO<sub>3</sub> as the result of CO<sub>2</sub> presence in solution will increase the corrosion rate in two ways; dissociation of H<sub>2</sub>CO<sub>3</sub> providing H<sup>+</sup> ions, and direct reduction of H<sub>2</sub>CO<sub>3</sub> through Equation 5 [1].



Nesic et.al proposed model of steel corrosion in aqueous CO<sub>2</sub> at various pH [3]. Based on their works, it was concluded that at low pH system (pH < 4), H<sup>+</sup> reduction is the dominant reaction due to high concentration of H<sup>+</sup>. At intermediate pH (4 ≤ pH < 6), both H<sup>+</sup> and direct H<sub>2</sub>CO<sub>3</sub> reduction were considered to be dominant.

In the literature review written recently by Nesic [6], Gray et.al also suggested that in CO<sub>2</sub> solutions at higher pH, direct reduction of bicarbonate ion becomes significant as the concentration of bicarbonate increases with pH. On the other hand, it has been observed that corrosion rate decreases with pH in the range 4 < pH < 7, while the concentration of bicarbonate increases, which is in contrary with the previous assumption. At higher pH and very low CO<sub>2</sub> partial pressure, direct reduction of water (Equation 6) becomes the dominant cathodic reaction [3]:



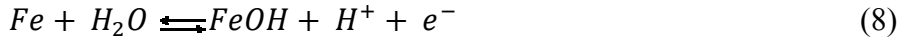
However, mechanism of H<sub>2</sub>CO<sub>3</sub> direct reduction has not been well defined. Schmitt and DeWaard & Milliams suggested that H<sub>2</sub>CO<sub>3</sub> adsorbs and reacts on the electrode [4].

### 2.1.2 Anodic Reactions

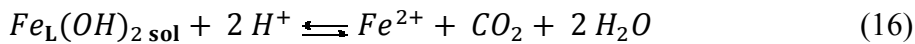
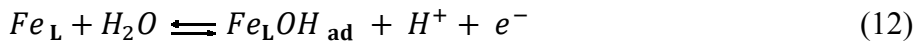
The anodic reactions in CO<sub>2</sub> corrosion of carbon steel is iron dissolution represented by Equation 7.



The mechanism proposed by Bockris et.al [7] has been studied and used by other researcher including deWaard and Milliams in investigating the cathodic reaction mechanism. In a strong acid condition, the reactions are described in Equation 8 – 10, with Equation 9 as rate determining step.



However, more recent study conducted by Nestic et.al. [5] showed that the mechanism could not be applied to all conditions. In addition, they proposed new mechanism based on solution pH. In their study, they reported that different kinetics of anodic iron dissolution in aqueous CO<sub>2</sub> is affected by carbonic species acting as a chemical ligand that plays important role in the reaction. The chemical ligand, Fe<sub>L</sub> (or Fe-CO<sub>2</sub>) is formed and adsorbed at the electrode surface (Fe<sub>L</sub>(OH)<sub>2</sub><sub>ads</sub>), and then catalyze the dissolution of iron by forming intermediate species (Fe<sub>L</sub>(OH)<sub>2</sub><sub>sol</sub>). At low ( pH<4) and intermediate pH (4<pH<5), the proposed mechanisms are shown in Equation 11 – 16 with Equation 15 as the rate determining step (rds).



At higher pH (pH>5), the mechanism is similar to those of lower pH but the determining step is Equation 13, instead of Equation 15.

### **2.1.3 Corrosion Damage**

CO<sub>2</sub> corrosion can cause both uniform corrosion and localized corrosion, such as pitting, mesa attack, and flow induced corrosion. The effect of flow has been proposed as the main factor causing localized attack [6]. In addition, environmental factors such as temperature, pH, CO<sub>2</sub> partial pressure, are also affecting the occurrence of localized corrosion. Pitting usually occurs at low velocities, and the susceptibility increases with temperature and CO<sub>2</sub> partial pressure. Likewise, mesa type attacks normally take place in low to medium flow. This type of damage is commonly found under the presence of iron carbonate film. Local breakdown of the corrosion film could cause a rapid mesa attack [8].

A flow-induced localized corrosion initially forms from pits or mesa attacks that propagate by local turbulence due to the pit geometry [9]. Experiments with video observation carried out by Nyborg et al. showed that mesa attack develops from localized corrosion beneath iron carbonate corrosion film [8]. This is followed by subsequent removal of the film by mechanical forces of the turbulent flow. Mesa attack grows stepwise laterally, and it looks like an area with bare metal where the whole corrosion film has been removed at the same time.

### **2.1.4 Factor Affecting CO<sub>2</sub> Corrosion**

There are two main factors affecting corrosion of steel in the presence of carbon dioxide; the characteristics of material, and environmental factors such as pH, temperature, solution chemistry, CO<sub>2</sub> partial pressure, etc.

#### **a) Steel Material**

Material properties comprise of chemical composition of the steel, heat treatment, and microstructural features. Some elements which are known to improve corrosion resistance of iron are chromium, nickel, copper, molybdenum, and also micro alloying elements like titanium. These elements act by promoting the

formation of a thin, impervious, oxide surface film or similar substance that protects the metal beneath from further attacks [10]. According to Al Hassan et al., chromium and molybdenum delayed and retarded the decomposition of martensite into ferrite and carbides upon tempering [11]. This less carbide structure has great reduction on corrosion rate because it hinders the potentially negative effects of carbides, i.e. galvanic coupling and local acidification. Videm et al. also found that corrosion resistance improvement on carbon steel with small amount of chromium addition was valid at high and moderate flowrate, under condition with and without carbonate film [12]. However, corrosion resistance can not only be related to chromium content only, but also on the carbon content and structure.

Heat treatment during manufacturing process is also found to have an important effect on the structure of steels produced, and eventually on their corrosion properties [10, 13]. It has been reported in various works that carbon steel with ferritic-pearlitic microstructure exhibit a better corrosion resistance compared to martensitic or martensitic bainitic microstructured steels [14-16]. In contrary, it is also found that the opposite condition where carbon and low-hardenable steel are most resistant when quenched and either tempered or double tempered to form martensite microstructure [17].

#### *b) pH*

The effect of pH on the CO<sub>2</sub> corrosion rate can be direct and indirect. Low pH is related to high H<sup>+</sup> concentration available to perform cathodic reaction in a corroding system. This in turn will affect the anodic iron dissolution on the other side. Nestic et al. on their study observed the reduction of corrosion rate at pH between 4 and 6, and addressed the phenomena to the general depletion of H<sup>+</sup> ions, which are required for the cathodic reaction (hydrogen reduction or direct H<sub>2</sub>CO<sub>3</sub> reduction) [18]. However the indirect effect of pH is considered to be the most important, especially on how pH change the solution chemistry and

conditions for formation of iron carbonate scale. An increase in pH results in a decreased solubility of iron carbonate that leads to increased precipitation rate and scaling tendency [6]. Other indirect effect of pH are increasing ratio of  $\text{Ac}^-/\text{HAc}$ , reducing the corrosion severity of acetic acid.

c) Temperature

Temperature in general accelerates the process involved in corrosion, such as electrochemical, transport, crystallization etc [6, 19]. Nevertheless, the effect of temperature is also influenced by pH where the  $\text{FeCO}_3$  film may form and reduce corrosion rate. Nesic summarized that at low pH where the precipitation of iron carbonate or other protective scales does not occur, corrosion rate increases steadily with temperature [6]. This effect can be related to the high solubility limit of  $\text{FeCO}_3$  and also the decrease in solution viscosity at higher temperature [3]. While at higher pH (more than 6), in the conditions where solubility of  $\text{FeCO}_3$  is low, an increase in temperature will enhance the kinetic of  $\text{FeCO}_3$  precipitation and protective film formation. Van Hunnik et.al proposed a model that predicts the increase in precipitation rate constant as a function of temperature [18, 19]. The precipitation rate constant is based on Arrhenius law, and defined in Equation 17.

$$k_r = e^{A - \left(\frac{B}{RT}\right)} \quad (17)$$

With  $A = 52.4$ , and  $B = 119.8$ .

Moreover, some previous works overlooked that the increase in temperature is always accompanied by the increase in water vapour pressure, and lower  $\text{CO}_2$  partial pressure respectively [18]. Consequently, according to Henry's law, the amount of dissolved  $\text{CO}_2$  in water is also decreased. Thus, the increase in temperature will increase the kinetics of precipitation, and also reduce the supersaturation of  $\text{FeCO}_3$  as a result of lesser amount of dissolved  $\text{CO}_2$  in the water.

d) CO<sub>2</sub> partial pressure

Effect of CO<sub>2</sub> partial pressure (P<sub>CO<sub>2</sub></sub>) is related to solution pH as well. In the condition where scale-free CO<sub>2</sub> corrosion occurs, the increase of P<sub>CO<sub>2</sub></sub> will increase the corrosion rate. This can be explained by the increment of H<sub>2</sub>CO<sub>3</sub> concentration as P<sub>CO<sub>2</sub></sub> increase that will lead to accelerated cathodic reaction [6]. At high pH, where FeCO<sub>3</sub> formation is favourable, the increase in P<sub>CO<sub>2</sub></sub> will increase bicarbonate and carbonate concentration, followed by higher supersaturation of FeCO<sub>3</sub>. High iron carbonate supersaturation enhances precipitation and scale formation. Nesic et al. [18] showed that when P<sub>CO<sub>2</sub></sub> is increased, pH at the surface initially increases due to corrosion and release of Fe<sup>2+</sup>, and then decreases since precipitation of FeCO<sub>3</sub> occurs rapidly. They also concluded that at constant pH, as P<sub>CO<sub>2</sub></sub> increases, FeCO<sub>3</sub> precipitation can increase faster than the corrosion rate.

e) Fluid velocity

The fluid velocity affects CO<sub>2</sub> corrosion rate by increasing the transport of species between steel surface and bulk solution. This is particularly relevant in corrosion without film formation where higher fluid velocity will increase corrosion rate. In the conditions with protective scales formed (higher pH), fluid flow may remove the film leading to an increase in corrosion rate [6]. However, as the main corrosion resistance in the presence of protective film is not only the species transfer but also the film layer itself; the effect of flow is not as great as in the condition without film formation. According to study conducted by Nesic et.al., reduction of H<sub>2</sub>CO<sub>3</sub> which is more pronounced at higher pH was found to be chemical reaction controlled and insensitive to flow [3]. In addition, the limiting current for the cathodic reaction is not controlled entirely by diffusion, but also by slow hydration of CO<sub>2</sub> that is not highly affected by the fluid velocity.

*f) Solution chemistry*

Ions that are present in the solution need to be taken into account since they may participate in the corrosion reactions. In the gas pipelines, condensed water commonly contains some carbonic species only. On the other hand, CO<sub>2</sub> corrosion of mild steel in oilfield is related to the presence of H<sub>2</sub>S, various organic acids, such as acetic acid, and dissolved salts [6]. Salts ions can combine and precipitate out of solution if their solubility limit is exceeded. Some examples of important salts in CO<sub>2</sub> corrosion are iron carbonate, calcium carbonate, and calcium sulphate. These precipitated salts also affect the corrosion rate. They could provide additional diffusion barrier between metal surface and corrosive medium, lowering part of the exposed steel area, and generate concentration gradient of the principal species involved in the electrochemical reactions (Fe<sup>2+</sup> and HCO<sub>3</sub><sup>-</sup>) [9]. The precipitation rate and protectiveness of the scale layer depend on the supersaturation in bulk solution. Solubility limits of most salts are functions of temperature and affected by the presence of other ions.

## **2.2 Corrosion Film Formation**

As mentioned previously, the scale precipitation in CO<sub>2</sub> corrosion can result in protective film that will reduce further corrosion rate. Review on previous works that had been done by Kermani et al., show that corrosion films in temperature range between 5°C to 150°C in CO<sub>2</sub> environment can be classified into transparent film, iron carbide film, iron carbonate film, and compound of iron carbide and iron carbonate film [9]. Details of each film type will be described in the following subchapter.

### **2.2.1 *Transparent Film***

This type of film is not thermodynamically the most stable corrosion product, with less than 1  $\mu\text{m}$  thickness and observed at room temperature [9]. The film does not contain carbonate, but only iron and oxygen in the proportion of 1:2, possibly  $\text{Fe}(\text{OH})_2$ . However, it is still debatable whether the ratio corresponds to Fe(II) or Fe(III). It is found that it has somewhat protectiveness against crevice and chloride pitting corrosion in similar manner to passivated stainless steel.

### **2.2.2 *Iron Carbide Film ( $\text{Fe}_3\text{C}$ )***

Iron carbide (i.e., cementite) is not a corrosion product. It exists in the scale as a result of its presence in the original steel microstructure, and accumulates on the surface after preferential dissolution of ferrite,  $\alpha\text{-Fe}$  into  $\text{Fe}^{2+}$  [2, 11]. As reported by Llongueras et al., experimental works also showed that formation of  $\text{Fe}_3\text{C}$  from iron and carbon dioxide is not thermodynamically favourable at room temperature [2]. The structure of iron carbide is described as a brittle, porous sponge layer [12].  $\text{Fe}_3\text{C}$  is electrically conductive and can affect corrosion process in several ways [9, 12, 14, 16, 20, 21]:

#### **a) Galvanic coupling**

$\text{Fe}_3\text{C}$  has lower overpotential compared to iron, thus galvanic contact between the two can speed up the dissolution of iron by accelerating the cathodic reaction. The high corrosion rate during pre-corrosion can be attributed to the gradual enrichment of uncorroded carbide at the steel surface. As iron corrodes, carbide particles will protrude from the surface, providing additional surface area for the cathodic reaction. This process will continue and decelerate when the carbide are undermined by corrosion scale and loose electrical contact with the steel.

b) Local acidification

Since the cathodic reaction occurs preferentially on the carbide, and because of its porous structure, water compositions in the vicinity of the region are changed. The aqueous medium at cathodic sites is becoming more alkaline, and that at the anodic sites is more acidic. This process will lead to local acidification in the aqueous medium trapped within the porous layer that eventually enhances steel corrosion.

c) Fe<sup>2+</sup> enrichment

The galvanic coupling that is mentioned above results in the increase of iron dissolution. This will increase the local concentration of Fe<sup>2+</sup> ions in the cavities/porous layer of the carbide. The supersaturation of Fe<sup>2+</sup> concentration will facilitate the formation of FeCO<sub>3</sub> that is corrosion protective.

d) Film anchoring

Local flow stagnation and higher local concentration of Fe<sup>2+</sup> within the porous carbide leads to FeCO<sub>3</sub> formation between the cavities. Lamellar structure of carbide provides better grip and helps to anchor FeCO<sub>3</sub> scale. In corrosion film consists of combination between FeCO<sub>3</sub> and Fe<sub>3</sub>C, there is improved tolerance on mechanical shear at higher flowrates, leading to reduced local corrosion.

Morphology of Fe<sub>3</sub>C is highly affected by microstructure of the steel. It has been reported that all carbon in normalized ferritic-pearlitic steel is bound as carbide [21]. Carbide that contributes to corrosion protection has lamellar form protruding out of the corroding steel surface. The schematic drawing is shown in the Figure 1.

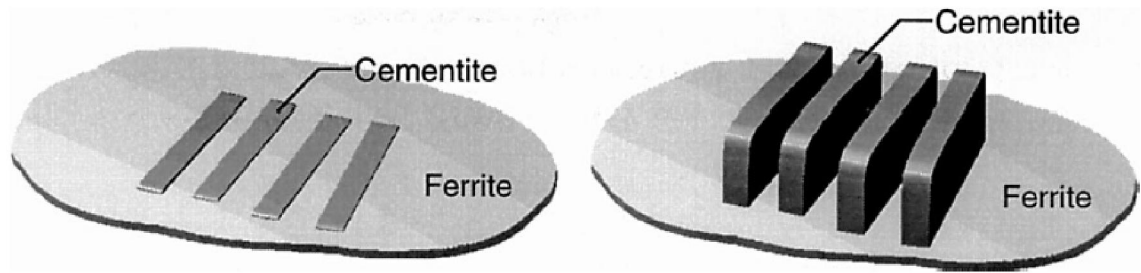


**Figure 1.** Schematic drawing of carbide (cementite) lamellas and the surrounding corroding ferritic-pearlitic steel (left is freshly ground surface, and right is corroded surface). Nyborg, et al. [21]

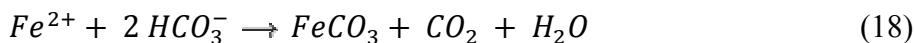
The carbide lamellas are skeleton-like structure sitting in the ferrite matrix of steel microstructure. They provide anchoring framework for the development of the corrosion protective layer. Ueda et al., through his work discussed that homogenous dispersed-carbide in steel N80 did not provide anchoring site as lamellar carbide in steel J55 [16]. Steel N80 has martensitic microstructure with the homogenous dispersed-carbide. The corrosion film formed on that type of carbide is easier to be pelled-off partially due to the absence of the anchoring effect. Steel with this characteristic exerts severe corrosion. The difference on morphology of carbide is of importance in the corrosion film protection.

Size and distribution of carbide particles are affected by heat treatment of steels. In tempered martensite, the increase of tempering temperature in the temperature range where  $Fe_3C$  starts to precipitate and coarsen, will result in the decrease of corrosion rate [17]. In martensitic structure,  $Fe_3C$ /ferrite interfacial seems to be important parameter controlling corrosion rate. The decrease in  $Fe_3C$  surface area because of coarsening leads to the decrease in corrosion rate. In ferritic-pearlitic steel, the effect of  $Fe_3C$  size and distribution in corrosion rate of steel is less regular. According to Mishra et al., higher corrosion rate was predicted when distribution of pearlite in ferrite matrix is more uniform and the interfacial area between the phases is higher (as in normalized carbon steel), than in a banded structure of ferrite and pearlite (as in annealed carbon steel) [17]. Dugstad et al. conducted experiments on St-52 steel that originally has ferritic-pearlitic structure

with carbide bands [15]. The steel under their observation underwent various different heat treatment such as quenched, tempered, and spherodized. Carbide grains were visible after tempering the steel at 650°C. On the other hand, spherodizing changed the structure and distribution of carbide slowly. Steel with smaller and more homogeneously distributed carbides was observed after 24 hr spherodizing. It is found that with increasing tempering temperature followed by quenching, smaller carbides will be formed. These small carbides particles have tendency to stick together and form networks. This phenomenon has two different effects. If FeCO<sub>3</sub> film is able to form within the network, the corrosion rate is low in the absence of mesa attack. Conversely, if there is no or little FeCO<sub>3</sub> precipitates in the carbide network, smaller carbides particle leads to higher surface area for cathodic reaction, thus higher corrosion rate.

### 2.2.3 *Iron Carbonate Film*

FeCO<sub>3</sub> film can grow in sweet environment, and may precipitate not only on the steel but also directly on the Fe<sub>3</sub>C. This film has protective effect on corrosion of the steel by its coverage and adherence structure which then limits the electrochemical activity. The adherence and thickness of FeCO<sub>3</sub> scale depends on the metal microstructure. Precipitation of FeCO<sub>3</sub> film can be simplified as in Equation 18 [20].



Precipitation of crystalline films proceeds through two phases, nucleation and crystal growth. It is believed that for FeCO<sub>3</sub> precipitation, the nucleation phase is very fast, leaving the crystal growth phase as the controlling step [19, 22]. Dugstad proposed a mechanism where nucleation rate increases exponentially with relative supersaturation, while the crystal growth is linearly related with this parameter [23]. Thus, crystal growth rate will predominate at low supersaturation, and the nucleation will be dominating at high supersaturation. The overall process

is affected by some parameters, such as solution chemistry, temperature, and pH. Solution chemistry is the most important factor since supersaturation of iron carbonate is the main requirement for the scale to be formed. Supersaturation is defined in Equation 19.

$$S = \frac{[Fe^{2+}][CO_3^{2-}]}{K_{sp}} \quad (19)$$

Temperature has two effects on the precipitation of FeCO<sub>3</sub>. First it affects the solubility product of the salt which will also affect the supersaturation value. In contrary to most of other salts, the solubility limits of iron carbonate decreases as temperature increases. Sun et.al. proposed equation that relates solubility limit as function of temperature and ionic strength based on the literature data as expressed in Equation 20 [24].

$$\log K_{sp} = -59.3498 - 0.041377 T_k - \frac{2.1963}{T_k} + 24.5724 \times \log(T_k) + 2.518 I^{0.5} - 0.657 I \quad (20)$$

where K<sub>sp</sub> is the solubility product, T<sub>k</sub> is temperature in Kelvin, I is ionic strength in mol/L.

Second effect of temperature is to the FeCO<sub>3</sub> crystallization rate. Johnson and Tomson conducted a study to investigate the growth rate of FeCO<sub>3</sub> crystal, which was found to be extremely temperature sensitive [25]. Van Hunnik et al. suggested that the precipitation kinetic modelled by Johnson and Tomson does not apply to a wide range of supersaturation level, since it was fitted on low supersaturation level (S<2). They proposed new equation on iron carbonate precipitation kinetic as written in Equation 21 [19].

$$[Fe^{2+}]_{prec} = k_r \frac{A}{V} K_{sp} (S - 1)(1 - S^{-1}) \quad (21)$$

with k<sub>r</sub> is temperature-dependent rate constant, A/V the surface/volume ratio, K<sub>sp</sub> the solubility product of FeCO<sub>3</sub>. The value of k<sub>r</sub> at different temperature is found to increase with increasing temperature as explained in Equation 17.

From those two effects, it is clear that temperature plays important role in iron carbonate formation. At high temperature ( $T > 60^{\circ}\text{C}$ ), the precipitation proceed faster while supersaturation is low. This condition will result in dense crystalline film with good protectiveness. At low temperature ( $T < 40^{\circ}\text{C}$ ), less precipitation occurs, and the supersaturation is high due to accumulation of dissolved iron carbonate. Consequently, corrosion film will be porous, loosely adherent, and has low crystallinity. This type of film is less protective than those formed at high temperature [23].

Other parameter that influences the formation of iron carbonate film is pH. Increase in pH results in decreased solubility of iron carbonate and increased supersaturation. All of these conditions may result in higher precipitation rate and surface scaling tendency [6, 22].

#### ***2.2.4 Iron Carbonate plus Iron Carbide Film***

This is the most common type of film found on carbon and low alloy steel in  $\text{CO}_2$  corrosion environment. Corrosion protective characteristic of the film depends on when and where iron carbonate precipitates. The differences between protective and nonprotective film is in the presence of empty  $\text{Fe}_3\text{C}$  film formed directly on the steel surface as illustrated in Figure 2. In protective film,  $\text{FeCO}_3$  precipitation takes place directly on the metal surface and integrates with  $\text{Fe}_3\text{C}$  phase. While in nonprotective film, initial formation of  $\text{Fe}_3\text{C}$  layer on the metal surface is followed by partial  $\text{FeCO}_3$  sealing close to or beyond the external limit of  $\text{Fe}_3\text{C}$ .

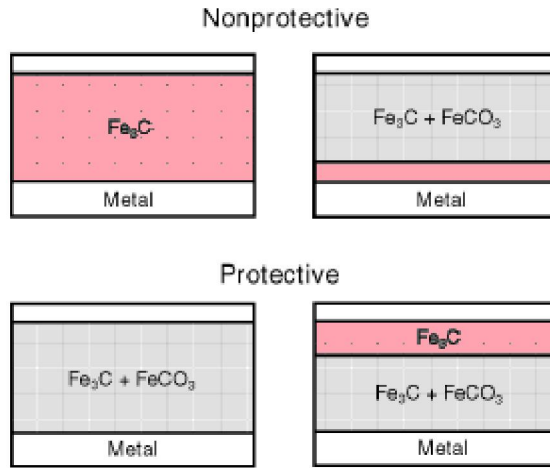


**Figure 2.** Different morphologies observed for protective and nonprotective corrosion layer. Crolet, et al. [20]

In order to obtain protective film, the growth rate of iron carbonate must be equal or higher than the corrosion rate. Otherwise, there will be gap between steel surface and iron carbonate filled part of the film, since corrosion still proceeds under the film [22, 23]. Concept of scaling tendency has been introduced in several works and it is defined in Equation 22 as the ratio between precipitation rate and corrosion rate [19, 22].

$$ST = \frac{R_{FeCO_3}}{CR} \quad (22)$$

where  $R_{FeCO_3}$  is precipitation rate of iron carbonate, and CR is corrosion rate.

Scaling tendency has critical value, termed as critical scaling tendency, at which the effective protection by iron carbonate film precipitation starts. Below the critical value, the rate of precipitation is far lower compared to the corrosion rate. This will result in porous and unprotective films. On the other hand, above the critical value, the precipitation rate is higher than the corrosion rate, leading to dense and protective iron carbonate film. However, the consideration of scaling tendency should be applied at the steel surface, where film forms [22]. Solution chemistry at the vicinity of steel surface might be very different from the bulk solution, especially in the presence of other films type (e.g. iron carbide, oxide,

surface mills). It is also found that critical scaling tendency decreases when the carbon content in the steel increases [19]. The reason is because carbon steel with high carbon content (more than 0.15%) can form cementite/carbide network which remains on the surface after corrosion of ferrite phase. The network will result in higher local supersaturation level, leading to protective film formation at lower bulk supersaturation.

Main parameters that enhance the formation of protective film are any barrier that restricts transport of reaction products from the surface and anchoring properties of steel surface. Therefore, metal surface with oxide layer is less susceptible to corrosion compared to freshly ground surface [23]. However, the exact role of oxide film is not clear whether it acts as initiator for iron carbonate protective film or as the main part in keeping the corrosion rate low for a long term. Fluid turbulence can increase transport of  $\text{Fe}^{2+}$  ions away from steel surface, and  $\text{H}^+$  toward the surface. This will result in internal acidification, and at the same time lowering supersaturation at steel surface. Iron carbonate precipitation will be slow, resulting in grain formation and voids, which is characteristic of less protective film [2, 22].

Regarding to the anchoring properties, Dugstad found that quenched and tempered low carbon steels need to be triggered with stagnant or semi dry period in order to initiate deposition of iron carbonate. Nonetheless, after the initiation step, there is almost no difference between these steel types [23]. The anchoring properties also related to the presence and morphology of carbide phase, which is believed to strengthen the iron carbonate film, and anchors it to the steel surface [15]. As described in the previous subsection, carbide is originated from the steel, so that microstructural aspect of the steel plays significant role.

Lopez et.al. conducted a review on effect of microstructure and chemical composition of carbon and low alloy steels in  $\text{CO}_2$  corrosion [26]. They concluded that microstructure and chemical composition are dependent variables which are related to each other. In addition to chemical composition, final microstructure of

a steel is also affected by thermomechanical treatment that being used during the production process [15].

Hassan et.al. found that X-65 steel that was quenched and tempered in the range of 350°C to 450°C corroded at higher rate compared to the as received steel in the beginning, but steady over the period of experiment (800 hours). While as received steel corrosion rate was increasing and became higher in the final condition. They addressed the phenomenon to the carbide particle size that becomes coarser as tempered temperature is increased. Coarse particle have smaller surface area compared to fine particles, giving less contact between the steel surface and solution. They also concluded that alloying elements such as chromium and molybdenum in carbon steel increased the time required for austenite to decompose into ferrite and/or a ferrite-Fe<sub>3</sub>C mixture. The alloying elements retarded decomposition of martensite into ferrite and carbides upon tempering. The lower carbide content will reduce the corrosion rate since iron carbide may enhance steel corrosion by acting as cathodic sites. On the other hand, Dugstad et.al. indicated that chromium has more effect on the corrosion resistance than the microstructure [15]. Eventhough the mechanism is not well defined, it is assumed that chromium improves mechanical strength of the protective film. Kermani et.al. also observed that chromium content has minimum concentration in order to have improved corrosion resistance [27]. Chromium should be at least 3% for the corrosion protective film to be stable and can grow at low pH (5).

### **2.3 Corrosion Control using pH Stabilization Method**

It has been explained that corrosion rate can be reduced under the presence of protective iron carbonate film. One of the corrosion prevention methods that utilize the protectiveness of this corrosion film is pH stabilization. The idea of pH stabilization is to achieve conditions that promote the formation of protective iron carbonate film. When protective iron carbonate formed on the steel surface, it acts

as a diffusion barrier for transport of reactants and corrosion products which governs the corrosion rate [28]. The characteristics of corrosion film such as porosity, thickness, and composition are determined by precipitation process, that eventually will affect its protectiveness. It has been explain in the previous subchapter, that protective iron carbonate film precipitation is controlled by supersaturation and temperature.

Since operating temperature is normally fixed, the desired condition for iron carbonate film precipitation can be accomplished by adjusting pH to optimum value. The pH should be in the range where supersaturations of iron carbonate concentration is high enough to form a dense and adherent film. In principle, pH stabilization is based on the reactions shown in Equation 23 and 24 [29] :



By adding base or increasing OH<sup>-</sup> concentration, the H<sup>+</sup> concentration needs to be adjusted in order to maintain correct water ion product (10<sup>-14</sup>). Thus, reaction 24 will take place to provide H<sup>+</sup>, and the amount of bicarbonate produced will be equal to the amount of added OH<sup>-</sup> in equilibrium.

Basically, any kind of bases can be used as pH stabilizer to increase the pH in the pipeline. In CO<sub>2</sub> system, the bases will form bicarbonate and carbonate ions apart from the alkalinity level [30]. Some chemicals that have been applied as pH stabilizer are organic bases such as MTBNa (mercaptobenzothiazole salt) and MDEA (methyldiethanolamine), due to its thermal stability. Strong base like NaOH (sodium hydroxide) has also been applied, but found to have harmful effect to the environment. NaHCO<sub>3</sub> (natrium bicarbonate) and Na<sub>2</sub>CO<sub>3</sub> (natrium bicarbonate) are relatively environmental safe, but require higher concentration compared to NaOH. In selecting pH stabilizer, it is important to take into considerations these operational issues [30]:

- Solubility: Solubility of pH stabilizer is influenced by the type of hydrate preventer, concentration of other salts, and also operating temperature. Solubility data of  $\text{NaHCO}_3$  and  $\text{Na}_2\text{CO}_3$  in MEG, DEG, and methanol can be found in other source [30].
- Compatibility: Injection of other chemicals in the process e.g. emulsion breakers, scale and foam inhibitor can accumulate in the glycol loop, and may interact with pH stabilizer. The compatibility with other chemicals needs to be ensured to avoid unwanted products that could create operational problems.
- Environmental impact: Introduction of pH stabilizer to environment can take place during transportation, injection, or carryover to other part of processing system. Thus, it is important to select chemical with minimum adverse effect to the environment.
- Heat stability/degradation: Glycol and pH stabilizer can be decomposed due to high temperature and oxidant contaminant such as oxygen. Temperature that limits chemical selection is glycol regeneration system temperature, and commonly it is in the range of 120 – 140°C. Even though oxygen ingress into the closed system of the process is possible, it is usually low and do not affect pH. However, it may produce foam and foulant that can clog in filter and coalescer.
- Loss of pH stabilizer: Loss of stabilizer into gas phase is considered to be negligible. If organic acids are present they will neutralize pH stabilizer leading to replenishment.
- Regeneration: pH stabilizer is commonly regenerated along with hydrate preventer (MEG or DEG). The loss in regeneration system depends on vapour pressure, temperature in pipeline and boiler, design and efficiency of condenser.

In spite of its effectiveness and efficiency, application of pH stabilizaton is limited by the occurrence of aquifer water breakthrough [29]. The presence of calcium ions in the formation water will impose the facilities into calcium carbonate scaling problem. Hence, it is necessary to take into account the produced water quantity and setting the tolerable limit in designing pH stabilization system.

Dugstad et.al. have compiled data on some fields that apply pH stabilization method to prevent corrosion that is summarized in Table 1 [30]. The method has been applied in many sweet systems, commonly combined with hydrate prevention by MEG injection into wellstream.

**Table 1.** Overview of some fields where pH stabilization has been applied [30]

Pipeline	Diameter/ Length	Year	pH Stabilizer	Max. Temp (°C)	Max. PCO <sub>2</sub> (MPa)	Max. Glycol (%)
Italiana Mineraria	10"/12 km	1973	MTBNa + inh.	50	0.17	70-80
Petroland (Netherlands)	-	1979	MTBNa + inh.	75	0.07 - 0.31	80
Pecorade, glycol contactor	-	1982	MTBNa	15% H <sub>2</sub> S + 9%CO <sub>2</sub>		
Heimdal MEG loop	-	1987	MDEA	40	0.03 - 0.04	80
Lille Frigg	10"/21 km	1994	MDEA	90	1	80
Froy Gass	12"/32 km	1995	MDEA	30	0.09	80
Troll – Kollsnes	36"/66 km	1997	NaHCO <sub>3</sub>	50	0.04	90
MENSA	12"/100 km	1997	MEA	60	0.04	75
Huldra	20"/150 km	2001	Alkyl Amine	50	0.4	79
Asgard A-B	-	2001	KHCO <sub>3</sub>	-	-	-
South Pars	-	2002	MDEA	-	-	-

### 3. EXPERIMENTAL METHOD

The purpose of this experiment was to find the effect of temperature, bicarbonate, and MEG concentrations as variable parameters in CO<sub>2</sub> corrosion of pre-corroded carbon steel. Experimental matrix summarizing the value of variable parameters is shown in Table 2.

**Table 2.** Experimental matrix

No	Temperature (°C)	MEG (%wt)	HCO <sub>3</sub> <sup>-</sup> (mmol/kg)
1	20	0	0
2			15
3			100
4		25	0
5			15
6			100
7		50	0
8			15
9			100
10	40	0	0
11			15
12			100
13		25	0
14			15
15			100
16		50	0
17			15
18			100

### 3.1 Test Specimen and Solution Preparation

To find the effect of different steel type, there were two specimens tested in the experiment; steel X-65 and St-52. Microstructure of both steels is ferritic-pearlitic, with the compositions as given in Table 3.

**Table 3.** Elemental analysis (%wt) of steel specimen (from certificate)\*

Steel Type	X-65	St-52
C	0.08	0.13
Si	0.25	0.38
Mn	1.54	1.29
S	0.0001	0.008
P	0.019	0.015
Cr	0.04	0.07
Ni	0.03	0.09
V	0.045	0.035
Mo	0.01	0.01
Cu	0.02	0.34
Al	0.038	0.05
Sn	0.001	0.015
Nb	0.043	-

\*) See Appendix A

The specimen was shaped as a cylinder with 1.00 cm diameter and 1.00 cm height, resulting in total exposed area as large as 3.14 cm<sup>2</sup>. The sample was drilled in the centre to create a hole in order to mount it in a working electrode holder as shown in Figure 3. The sample holder is made of threaded rod steel covered with epoxy tube.

Sample preparation comprised of grinding with 1000 mesh SiC paper, then degreasing by immersion in isopropanol for 5 minutes, and weighing after letting it dry for 15 minutes. To minimize accumulation of oxidation product and dirt on the surface of polished sample, after the sample was mounted in a sample holder,

it was flushed with ethanol followed with distilled water just before introduced to the solution.

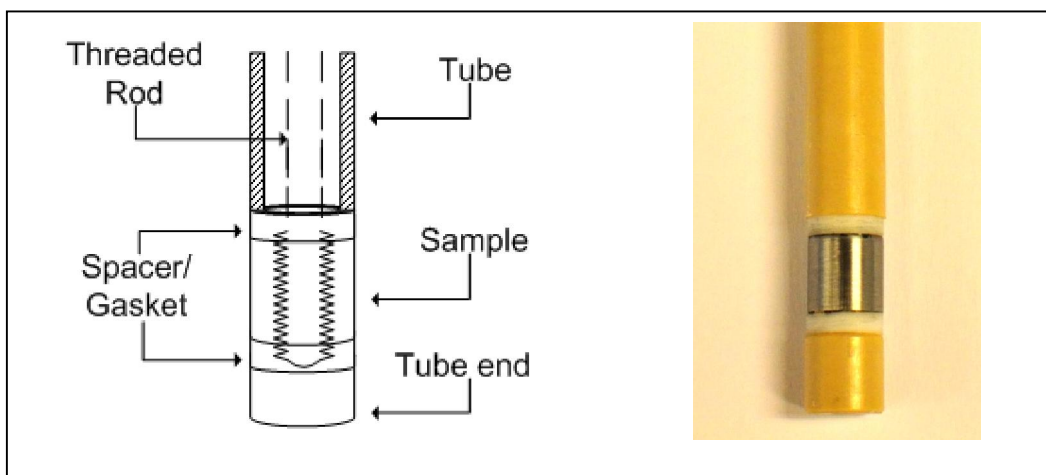


**Figure 3.** Sample mounted in working electrode holder

Electrolyte used in all experiment has NaCl concentration of 1 %wt, with MEG and  $\text{HCO}_3^-$  composition as listed in Table 2. Chemicals that are used to make solutions consist of:

- a. Distilled water
- b. MEG (as received), with specification:
  - Main compound : 1,2-Ethandiol ( $\text{C}_2\text{H}_6\text{O}_2$ )
  - Purity : > 97%
  - Supplier : VWR International AS
- c. NaCl, GR for analysis from Merck
- d.  $\text{NaHCO}_3$ , GR for analysis from Merck

The chemicals were mixed thoroughly, and the solution was let to sit overnight before being used. Solution volume in each experiment was 2 L, which is relatively large compared to the exposed surface of working electrode. Thus, it can be assumed that deposition of corrosion product in the solution is low.

### 3.2 Equipment Set Up

Experiments were conducted in a glass cell with three electrode configuration, consisted of reference electrode, counter electrode, and steel sample as working electrode. The reference electrode was K401 saturated calomel electrode (SCE) from Radiometer Analytical. Before and after each experiment, the potential of reference electrode was measured to get the idea of measurement drift. It was also checked before each usage to ensure that it was filled with saturated KCl solution. Some KCl crystal grain should also visible inside the electrode tube. In case the reference electrode needs KCl refilling, it was allowed to stabilize for minimum 12 hours before being used.

The counter electrode was M241Pt platinum electrode from Radiometer Analytical. The counter electrode was cleaned thoroughly and ensured to be free from debris prior to each experiment. The working electrode was the sample mounted in the sample holder. A schematic drawing in Figure 4 illustrates the equipment set up for the experiment. The cell was covered with glass plate and sealed with rubber gasket. The glass cover has holes for the three electrodes, and spare holes for pH electrode and liquid sample withdrawal. All electrode fittings were tightened with Teflon tape, and unused holes were sealed with rubber stoppers to ensure no oxygen intrusion into the cell.

The cell filled with solution was purged with CO<sub>2</sub> gas supplied from Yara Praxair at atmospheric pressure for 2 hours prior to starting the measurements. This was done to saturate the solution and removing the oxygen. After the initial deaeration, solution pH was measured using pH electrode. Metrohm 827 pH Lab as a pH meter with AG 9101 pH glass electrode was used for measuring pH. The pH glass electrode was calibrated regularly before used, against buffer solution at pH 4.00 and 7.00 to ensure the reliability.

CO<sub>2</sub> gas was allowed to bubble into the solution during the test to keep the system deaerated. The idea was to create a positive pressure inside the cell so that oxygen

from air would not be able to enter the system. To adjust system temperature to a level above room temperature, a water bath with thermostat was utilized.

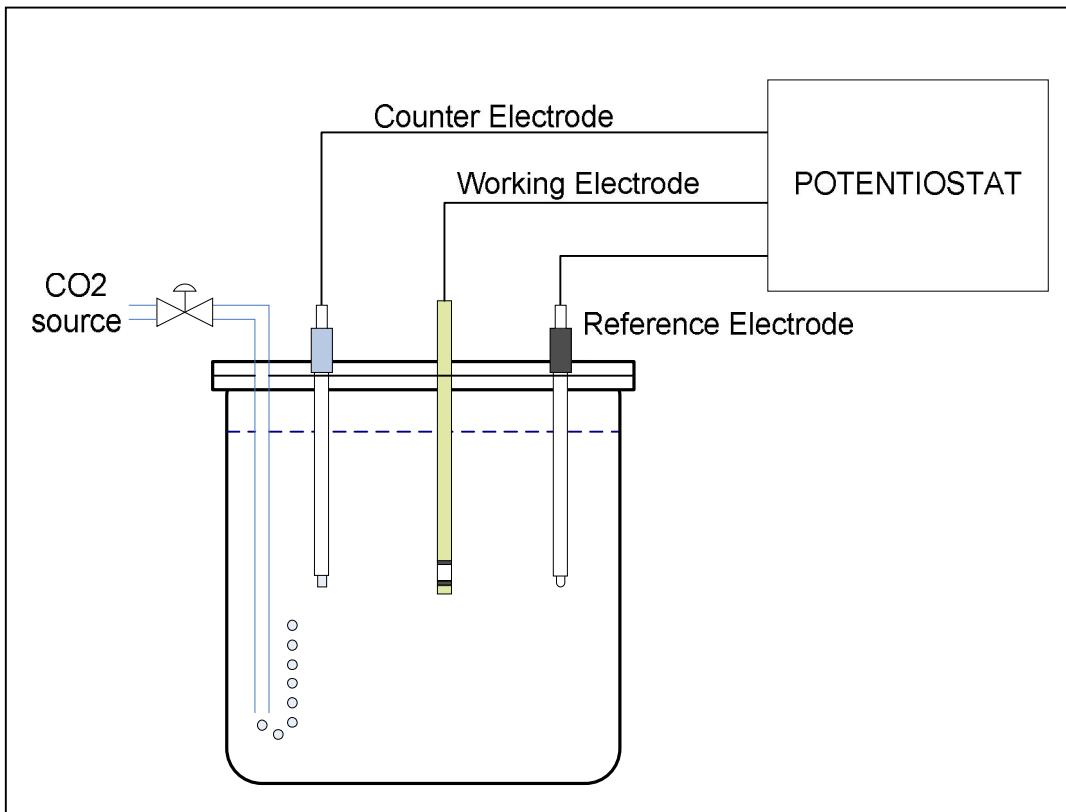


**Figure 4.** Equipment set up

### 3.3 Potentiostat

A potentiostat Gamry PCI4-300 from Gamry's Instrument was used for the tests and it was connected with a computer for data acquisition. First test was to measure the open corrosion potential for 15 minutes, followed by a potentiodynamic cathodic sweep. After that, a galvanostatic by applying anodic current as a pre-corrosion step,  $R_p/E_c$  trend measurement, and potentiodynamic polarization were performed with parameters listed in Table 4. Between anodic galvanostatic and  $R_p/E_c$  trend measurement, potentiodynamic cathodic sweep was

carried out. In addition, liquid sampling for Fe<sup>2+</sup> measurement were done twice, short before and after Rp/Ec Trend measurement.

**Table 4.** Electrochemical test parameter

Test	Parameter	Value
Galvanostatic	Initial current	0.25 mA/cm <sup>2</sup>
	Final current	0.25 mA/cm <sup>2</sup>
	Duration	24 hours
Rp/Ec Trend	Initial potential	-5 mV vs E <sub>corr</sub>
	Final potential	+5 mV vs E <sub>corr</sub>
	Scan rate	0.05 mV/s
	Duration	6 hours
Potentiodynamic Sweep	Cathodic potential ramp	+5 mV to -300 mV vs E <sub>corr</sub>
	Anodic potential ramp	-5 mV to 150 mV vs E <sub>corr</sub>
	Scan rate	0.2 mV/s

### 3.4 Corrosion Rate Calculation

The corrosion rate calculation was done using Rp/Ec trend measurement result. In addition, results from electrochemical tests were also cross checked with weight loss and Fe<sup>2+</sup> analysis.

Rp/Ec trend measurement is based on linear polarization resistance method, which estimates corrosion rate using linear approximation of polarization behaviour at potentials near the corrosion potential. The method is based on assumption that polarizing current changes linearly with potential within certain range from the corrosion potential, usually between 10 to 20 mV [31]. The Stern-Geary

relationship in equation 25 expresses the change in potential as a function of the change in polarizing current.

$$R_p = \frac{dE}{di} = \frac{\beta_A \beta_C}{2.3 (\beta_A + \beta_C) i_{corr}} \quad (25)$$

$\beta_A$  and  $\beta_C$  are the anodic and cathodic Tafel slope in mV/decade,  $i_{corr}$  is corrosion current density in mA/cm<sup>2</sup>, and  $R_p$  is polarization resistance in milliohm.cm<sup>2</sup>. By plotting potential vs current on linear graph,  $R_p$  can be obtained from the slope of the curve (dE/di) near the corrosion potential, while Tafel constants can be obtained from potentiodynamic polarization plot or from literature. The value of Tafel constant used in this experiment was 120 mV/decade for both anodic and cathodic Tafel constant. In order to find corrosion rate, equation 24 is modified to yield equation 26 and 27 [32].

$$i_{corr} (mA/cm^2) = \frac{\beta_A \beta_C}{2.3 (\beta_A + \beta_C) R_p} = \frac{B}{R_p} \quad (26)$$

B is often referred as Stern Geary constant, and it has unit in volts.

$$CR (mm/y) = 3.28 \frac{i_{corr} M}{n \rho} \quad (27)$$

Where M is molecular mass of corroding species in gram/mol, n is number of electrons transferred by the corrosion reaction, and  $\rho$  is density of material in g/cm<sup>3</sup>.

### 3.5 Electrochemical Test Result Validation

#### 3.5.1 Iron Content Analysis

Iron content in solution was measured to ensure the reliability corrosion testing and to find out FeCO<sub>3</sub> supersaturation. Measurement of iron content was carried out using UV-vis spectrophotometry method, at wavelength 508 nm. An UVmini-1240 spectrophotometer from Shimadzu was employed for this quantitative analysis. Fe<sup>2+</sup> in sample reacts with developer solution containing 1,10-

phenantroline-1-hydrate, forming iron(II) phenantroline complexes with yellow/red colour that absorbed the light at particular wavelength to some extent.

Chemicals for making developer solution consist of:

- a. 2.2 grams of 1,10-phenantroline-1-hydrate, GR for analysis and redox indicator from Merck
- b. 6 grams of acetic acid 100% ( $\text{CH}_3\text{COOH}$ ), GR for analysis from Merck
- c. 4 grams of hydroxyl ammonium chloride ( $\text{NH}_2\text{OH}\cdot\text{HCl}$ ), GR for analysis from Merck
- d. 8 grams of anhydrous sodium acetate ( $\text{C}_2\text{H}_3\text{NaO}_2$ ), pro analysis from Riedel de-Haen AG
- e. Distilled water

The chemicals were mixed with distilled water which was added until the final volume of solution reached 2 L. To prepare sample for spectrophotometry analysis, 200  $\mu\text{L}$  of electrolyte was taken from cylindrical cell using an automatic pipette, and mixed with 10 mL of developer solution.

A standard calibration curve of the instrument was needed for calculation of iron concentration in sample. The curve was built by measuring spectra absorbances of a series of standard solution with known iron concentration. The standard solution was made from ammonium iron(II)-sulphate-6-hydrate which was mixed with developer solution. The correlation between the iron concentrations in standard solution with spectra absorbance was used for quantifying iron concentration in sample. Standard calibration curve can be seen in Figure B.1, Appendix B. When analysing iron in the sample, absorbance readout from spectrometer is fitted into the standard calibration curve to obtain iron concentration in sample.

### ***3.5.2 Weight Loss Measurement***

Weight loss measurement during experiment is used to validate the corrosion rate calculation from electrochemical test result. Before experiment was started, the

cleaned and polished sample was weighed to find the initial sample mass. Upon finishing the electrochemical testing procedures, the sample was taken out of solution, immersed in isopropanol for 5 minutes, let dry for 15 minutes, and weighed. The difference in sample mass before and after a set of electrochemical testing was the weight loss. The corrosion product deposited on the sample surface was not cleaned prior to weighing. However the trend in weight loss can be correlated to the corrosion rate in the sample at different variations of testing parameter. The calculation result on weight loss is summarized in Appendix D.

### **3.6 Surface Analysis using Scanning Electron Microscopy**

Surface analysis using SEM (Scanning Electron Microscope) was not performed to all samples due to its high cost and time consumption. The analysis was only performed to some samples that showed different behaviour in the electrochemical testing result, to find out if there is any surface change occurred as the result of pre-corrosion and corrosion process itself. The accelerating voltage used on SEM analysis was 15.0 kV, with 2500x magnification. Most of the samples surfaces were only analyzed using digital microscope with 100 – 300x magnification. A Leica Microsystem digital microscope CLS 150X was utilized for this purpose.

In preparing sample for SEM analysis, the sample must first be preserved with an epoxy coating made from a mixture of EpoFix resin and hardener from Struer. The mixture was prepared with a composition of 7:1 for the ratio of resin to hardener. It was then placed into a vacuum chamber to remove the entrapped air bubble that may reduce the epoxy quality. The sample should be immersed and fully coated with the epoxy mixture, and put in a vacuum chamber for several minutes. This was done in order to ensure an even coat layer on the surface of preserved sample. After that, the sample was heated in the oven at temperature 50°C for several hours to harden the epoxy coating. Since the sample was not directly analyzed after the surface preservation, it was stored in a desiccator.

## 4. RESULT AND DISCUSSION

The experiment result will be presented in this chapter classified by its operating temperature. Reference electrode used in the experiment was considered to have good stability since it was deviated 1.6 mV from the initial value at the maximum. Solution pH after 2 hours CO<sub>2</sub> purging was found to be highly dependent on bicarbonate concentration. In solution without bicarbonate, pH was on average 3.9. While in solution with 15 mmol/kg HCO<sub>3</sub><sup>-</sup>, the average pH was 6.2, and in solution with 100 mmol/kg HCO<sub>3</sub><sup>-</sup> the average pH was 7.

Temperature in the experiment seemed to have no effect on solution pH, while the increase in MEG concentration only slightly increased the solution pH. Highest pH was attained by 50% MEG solution, with the maximum difference of 0.4 compared to solution without MEG. Addition of MEG into solution is known to modify the solution properties, such as increased solution viscosity, decreased CO<sub>2</sub> solubility and diffusivity, decreased water activity, and decreased solution polarity [33]. The decrease of CO<sub>2</sub> solubility and diffusivity with the increase of MEG concentration in the solution results in lower H<sub>2</sub>CO<sub>3</sub> concentration, which may dissociate further into bicarbonate and carbonate ions while releasing H<sup>+</sup> ions. Thus, higher pH can be expected at high MEG concentration.

### 4.1 Corrosion Potential

Corrosion potential was measured short after the working electrode had been inserted into the cell. The value represents cell potential when no external potential and current applied to the cell. Measurements were done for 15 minutes, and results from X-65 and St-52 are shown in Figure 5. Corrosion potentials of both steels had similarity in trend regarding to solution pH. X-65 had slightly higher potential compared to St-52.

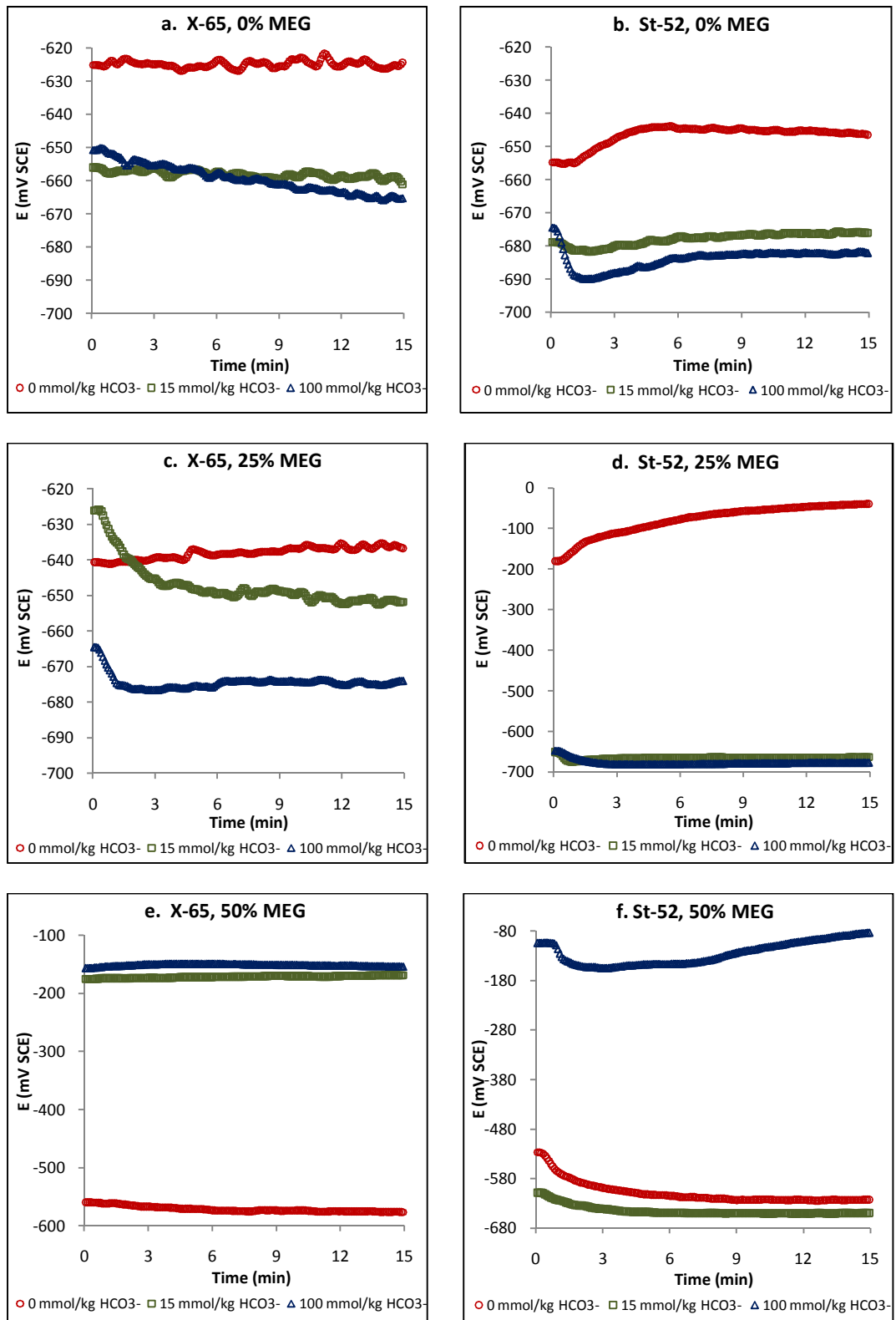


**Figure 5.** Corrosion potential of series 0-100 mmol/kg  $\text{HCO}_3^-$ , at 20°C

In 0% MEG and 25% MEG solution (Figure 5. a - d), the pH increase is followed by the shift of potential curve towards more negative value. Potential ranges between -620 mV to -690 mV, with the exception of series 0 mmol/kg  $\text{HCO}_3^-$  in 25% MEG which has potential of -40 mV (Figure 5.d).

Compared to lower MEG concentration (Figure 5. a – d), the stabilized potentials of various series with different  $\text{HCO}_3^-$  concentration are higher at 50% MEG (Figure 5.e – f). High viscosity and lower polarity of the solution due to MEG addition will affect the solvation of the ions participating in electrochemical reactions [33]. The retardation of corrosion can end up in high corrosion potential. It can be seen in Figure 5.e –f that curves in 50% MEG solution where both X-65 and St-52 steels have elevated corrosion potential at 100 mmol/kg  $\text{HCO}_3^-$ . In addition, this phenomenon was also occurred in series 15 mmol/kg  $\text{HCO}_3^-$  for X-65 (Figure 5.e).

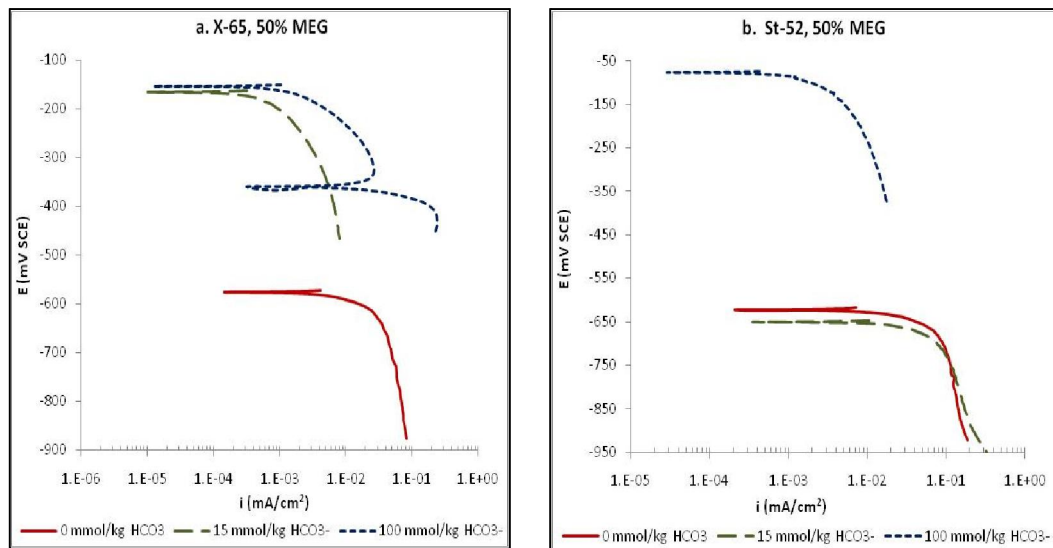


**Figure 6.** Cathodic potentiodynamic sweep of (a) X-65 and (b) St-52 in 50% MEG, 0-100 mmol/kg  $\text{HCO}_3^-$ , at 20°C

A cathodic potentiodynamic sweep that was done after the corrosion potential measurement is shown in Figure 6.a and b for series in Figure 5.e and f respectively. The sweep starts from corrosion potential, with scan rate of 0.5 mV/s. It can be seen that for steel X-65, series 100 mmol/kg  $\text{HCO}_3^-$  reached

another mixed corrosion potential at more anodic value. Complete result on cathodic potentiodynamic sweeps of other series can be found in Appendix B.

This corrosion potential measurement was done in the beginning of experiment, before any other electrochemical testing was performed. The sample was also freshly polished steel. In this case, no corrosion film either iron carbide nor iron carbonate was expected to form. In addition, the reference electrode reliability had always been maintained by performing regular checking prior to each experiment. The checking procedure includes ensuring that reference electrode is filled with saturated KCl solution, and KCl crystal grain can be seen inside the electrode tube. KCl solution refilling was done at least 12 hours before experiment, in order to allow the electrode to stabilize. So, there were no obvious reasons for deviations with high corrosion potential which were found early in the experiment.

However, some possible reasons that can cause the deviations will be proposed here. First, the irregularities in working electrode that has surface defects may cause variation in measurement. Sample preparation such as polishing might not be able to eliminate some of the surface defects. Secondly, despite of attempts to minimize lag time between working electrode preparation and introduction into electrolyte, oxide film might be formed on the surface of working electrode. This thin oxide layer that formed instantaneously when the steel contacted with air was the most possible reason. The oxide film could possibly cover the steel surface, and cause high corrosion potential.

Experiment results at 40°C are illustrated in Figure 7. The results show better trend compared to experiment at 20°C. Almost all of the series in various MEG concentrations has series 0 mmol/kg  $\text{HCO}_3^-$  with the highest corrosion potential, followed by 15 mmol/kg, and 100 mmol/kg  $\text{HCO}_3^-$  having the lowest potential. The stabilized potential values are similar for all series in X-65 and St-52 steels, ranges between -633 mV to -693 mV.

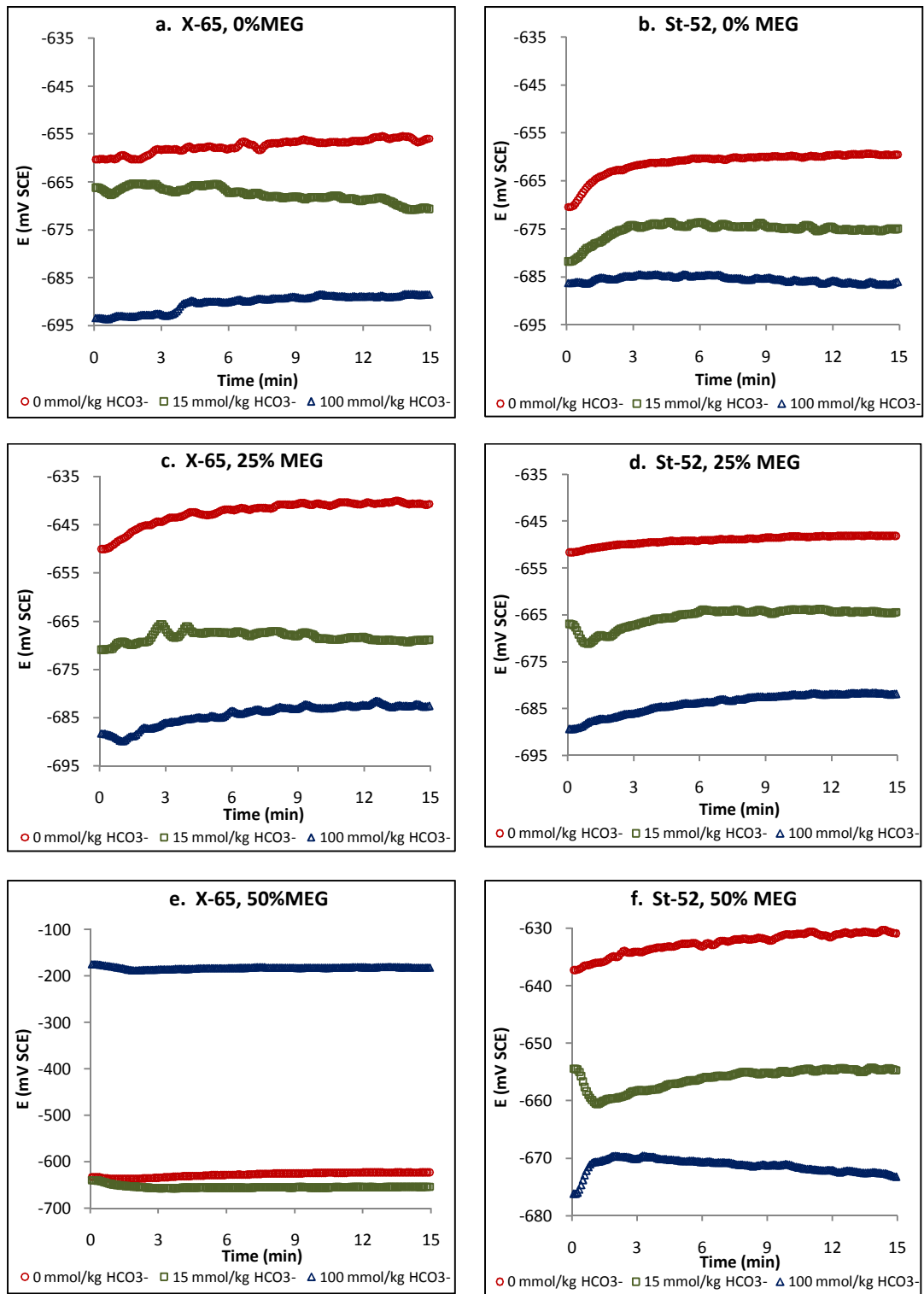


**Figure 7.** Corrosion potential of series 0-100 mmol/kg  $\text{HCO}_3^-$ , at 40°C

As in experiment at 20°C, more positive corrosion potential occurred with the increment of MEG concentration. The only series that showed deviation was X-65 in 50% MEG and 100 mmol/kg  $\text{HCO}_3^-$  solution (Figure 7 e). Some possible reasons that could cause this deviations have been explained. There was also evidence that high solution pH was found to encourage the occurrence of more positive corrosion potential, which was also happened in experiment at 20°C.

## 4.2 Galvanostatic Measurement

Anodic galvanostatic was performed on the cell in order to accelerate the corrosion on working electrode by applying constant current ( $0.25 \text{ mA/cm}^2$ ) for a period of 24 hours. The obtained potential with time of the working electrode is plotted in Figure 8 for experiment at 20°C. This electrochemical technique can be used to characterize process that occurred during normal corrosion in a shorter time.

Effect of the increasing MEG concentration on steel X-65 (Figure 8.a, c, e) was a slight potential increase on each series of  $\text{HCO}_3^-$  concentration. Series 15 mmol/kg  $\text{HCO}_3^-$  at 50% MEG which does not follow the trend shows that there was high noise during the first 2.5 hours of measurement. The source of noise was bad connection of the working electrode mounting on the sample holder. Over tightening or loosening the working electrode can result in noise during measurement. Nevertheless, after proper retightening the working electrode, measured potential still have very high value (-225 mV) compared to other series which stabilized in the range between -500 mV to -660 mV.

On the other hand, effect of various  $\text{HCO}_3^-$  concentrations showed different trends on the potential over time even though all were approaching steady value in the end of scanning period. In X-65, the potential shifted to a lower potential as pH increased. The only exception was series 15 mmol/kg  $\text{HCO}_3^-$  in 50% MEG solution which had noise and electrical connectivity problem.

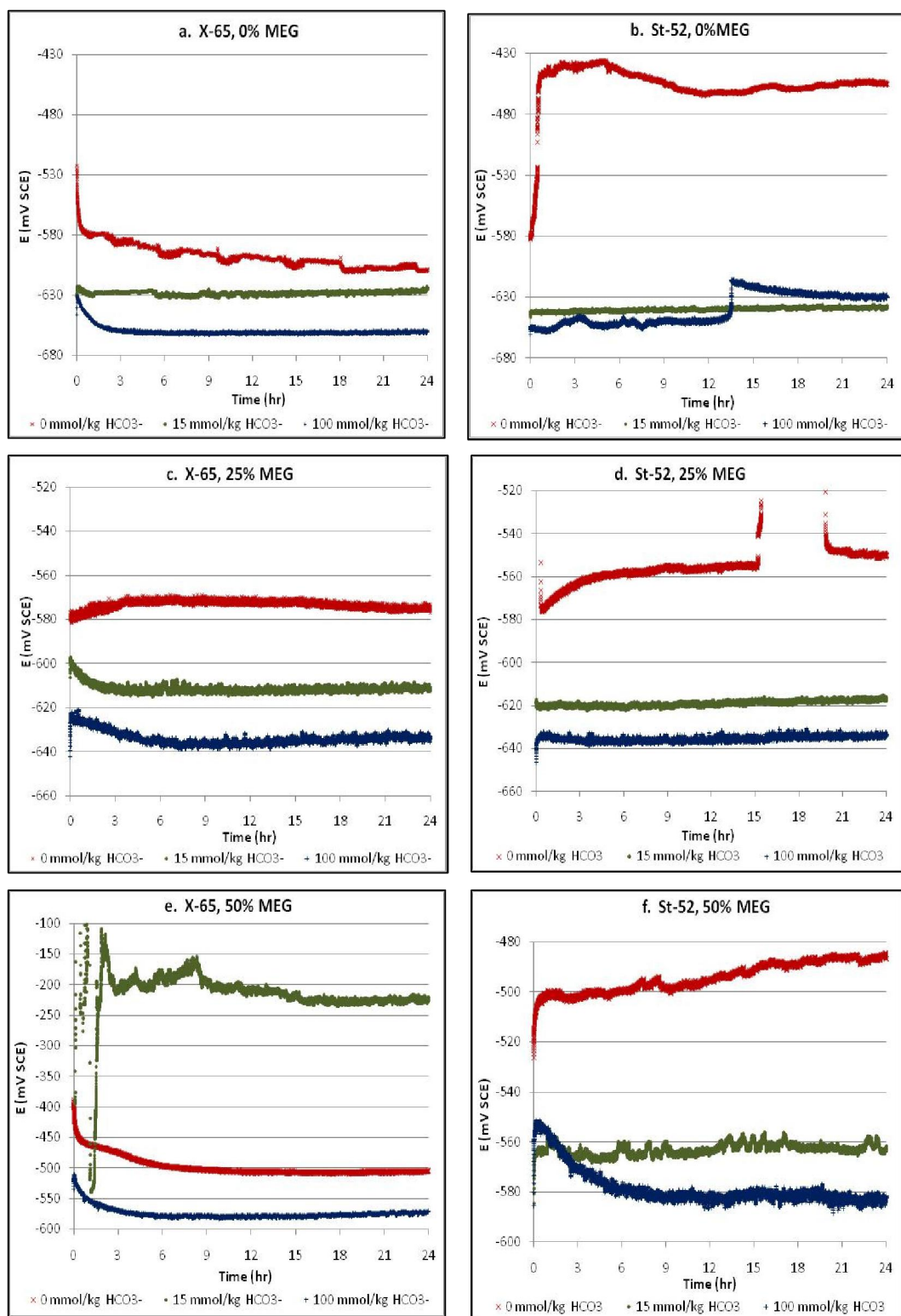


**Figure 8.** Potential under  $0.25 \text{ mA/cm}^2$  applied current of series 0-100 mmol/kg  $\text{HCO}_3^-$ , at  $20^\circ\text{C}$

In most of the curves, initially there was a sudden increase of potential which then decreased gradually. However, series 0 mmol/kg  $\text{HCO}_3^-$  in 25% MEG solution had a longer delay before the potential started to rise compared to other series. This increase in potential was caused by the formation of corrosion film as anodic reaction was forced to progress. The following gradual decrease in potential illustrated active corrosion of steel occurred. As the time went by, partial dissolution of corrosion film might take place leading to pore formation. These film formation and dissolution processes were competing and resulting in the potential oscillation with time.

Similar effects of MEG and  $\text{HCO}_3^-$  concentration were also found in steel St-52 (Figure 8. b, d, and f). Several deviations occurred on the experiment result of this steel type. Series 0 mmol/kg  $\text{HCO}_3^-$  showed the highest potential at solution without MEG (Figure 8.b). The potential rose steeply during the first hour, from -580 mV to -445 mV before decreasing to a steady value of -455 mV. The same series at 25% MEG had a lower potential than the one at 50% MEG as in steel X-65, although some noise occurred during measurement.

While in 50% MEG, potential of the series without bicarbonate increased with time even after passing the initial hump. High viscosity and low diffusivity of 50% MEG solution might reduce the corrosion film dissolution. The increasing potential over time also occurred on series 100 mmol/kg  $\text{HCO}_3^-$  in 0% MEG solution. It had a second maximum at 13.5 hours, in which the potential decreased afterwards. This shows that formation of protective corrosion film is dominant rather than dissolution process. However the final steady state potential of series 100 mmol/kg  $\text{HCO}_3^-$  was only 8 mV higher from series 15 mmol/kg  $\text{HCO}_3^-$ .

In St-52, all series with no  $\text{HCO}_3^-$  added at various MEG concentrations has relatively high potential compared to steel X-65. The steady potential from the scans varies from -455 mV to -635 mV, which is in the more positive range compared to steel X-65. Steel St-52 has higher carbon content compared to X-65. Higher carbon content can result in more carbide phase exposed to the surface as

corrosion was forced to progress. Carbide has a positive effect where it provides anchor for  $\text{FeCO}_3$ , which eventually may lead to more protective film formation. As the film formed and covered the steel surface, the corrosion potential is shifted to a more noble value [34]. However, this finding was quite surprising since protective  $\text{FeCO}_3$  film was not expected to form in series 0 mmol/kg  $\text{HCO}_3^-$ , due to the low pH (4) and temperature ( $20^\circ\text{C}$ ). The only source of carbonate ions was from  $\text{CO}_2$ . Nevertheless,  $\text{FeCO}_3$  will be formed on steel under  $\text{CO}_2$  corrosion as long as the steel surface reached supersaturation, even though the bulk solution was undersaturated.

Experiment with applied current of  $0.25 \text{ mA/cm}^2$  showed similar trends and steady-state potential for both steels (Figure 9). In contrary to the experiment result at  $20^\circ\text{C}$ , experiment at  $40^\circ\text{C}$  showed that the potential increased slowly with time except for series 100 mmol/kg  $\text{HCO}_3^-$ . Gradual potential increase indicated that  $\text{FeCO}_3$  film with better protectiveness was formed, and that the process was time consuming. Solubility of  $\text{FeCO}_3$  is a function of temperature, and high temperature results in lower solubility, which enhances the possibility of  $\text{FeCO}_3$  formation.

According to the hypothesis, series 100 mmol/kg  $\text{HCO}_3^-$  that attained higher pH should have its potential increased since there was more  $\text{CO}_3^{2-}$  needed for supersaturation, which might lead to film formation and surface modification. Conversely, Figure 9.a – d showed that the series decreased first and then increased after some time. Possible explanation is that at high pH and temperature where  $\text{FeCO}_3$  film is expected to form, initially,  $\text{Fe}_3\text{C}$  will form first followed by  $\text{FeCO}_3$  formation partially on the steel surface. This will create a galvanic cell with the surrounding bare steel leading to higher corrosion during the early period of the measurement. The protectiveness of  $\text{FeCO}_3$  will be determined by the scaling tendency, and depends on how fast the film formed compared to the steel's corrosion rate.

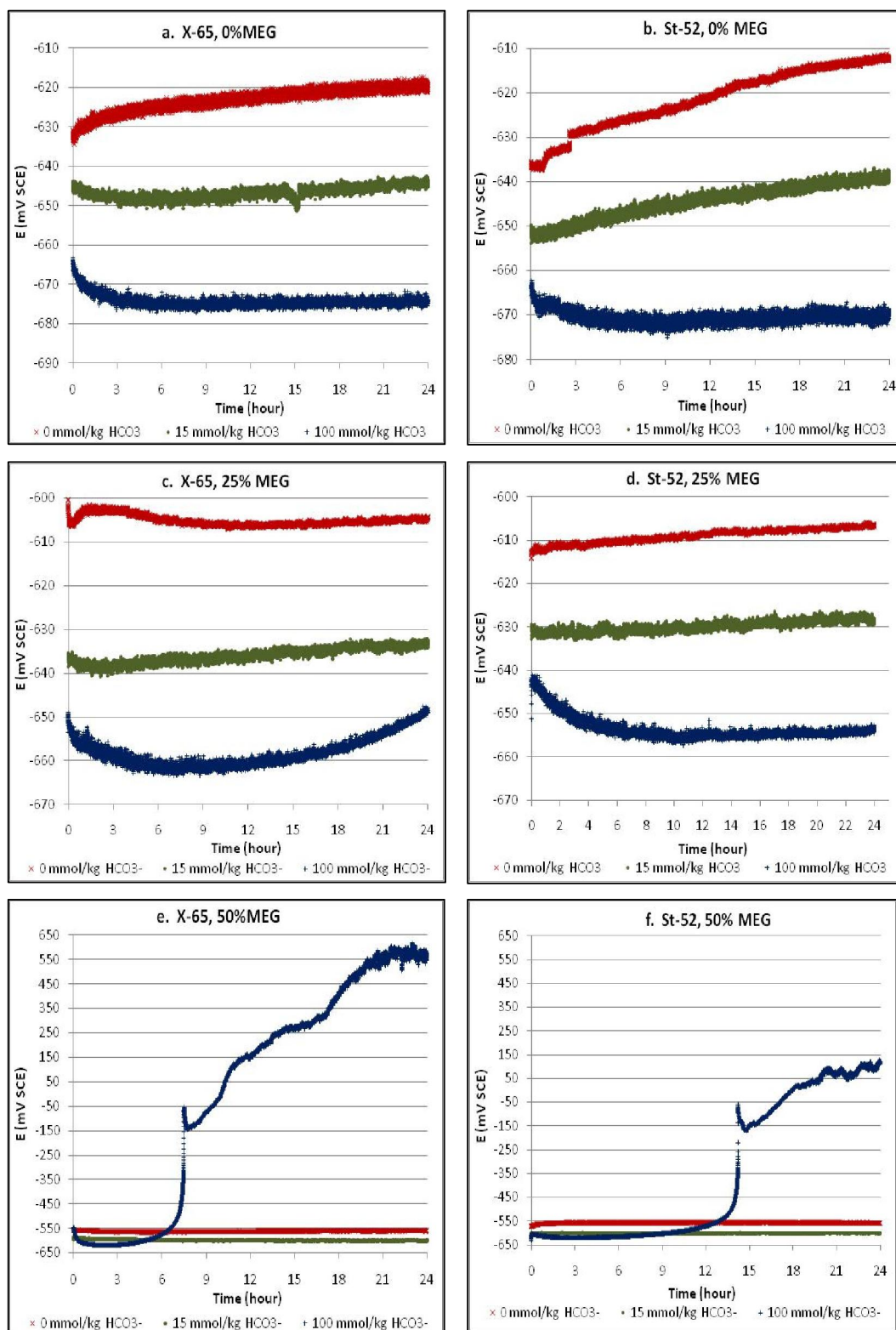


**Figure 9.** Potential due to  $0.25 \text{ mA/cm}^2$  applied current of series 0-100 mmol/kg  $\text{HCO}_3^-$ , at  $40^\circ\text{C}$

In 50% MEG solution (Figure 9.e and f), a sudden potential increase was observed in series 100 mmol/kg  $\text{HCO}_3^-$  for steels X-65 and St-52 after 7 hours and 14 hours respectively. According to some authors, this was an indication of steel passivation [34, 35]. Han et.al. proposed that formation of passive film is closely related with the presence of  $\text{FeCO}_3$  [34]. When iron carbonate becomes compact and able to retard replenishment of  $\text{H}^+$  on the steel surface, a high local pH is achieved leading to a passive film formation under  $\text{FeCO}_3$  layer.

There was also possibility of artifact on an insulating film where applied current of  $0.25 \text{ mA/cm}^2$  may cause a high potential on the Gamry's potentiostat in order to obtain this level of current. The same curve behavior was not observed in experiment with the same  $\text{HCO}_3^-$  concentration at  $20^\circ\text{C}$ . Therefore, at such low temperature  $\text{FeCO}_3$  film was not expected to form within the time frame despite of high pH. Nonetheless, potential increases of the series at  $40^\circ\text{C}$  were found to be very high, 550 mV for X-65 and 140 mV for St-52, all measured against SCE reference. These potential values were out of expected range, and the experiments should be redone in order to reassure the reliability of the results.

In order to find the potential increase contribution from MEG oxidation, an additional experiment was performed. Potentials were recorded under application of  $0.25 \text{ mA/cm}^2$  anodic current on an inert Pt electrode and various MEG concentrations to find out the potential increase from MEG addition. Similar condition such as continuous  $\text{CO}_2$  purging and temperature of  $40^\circ\text{C}$  was maintained. A gradual addition of MEG starting with 20% in the first addition, followed by 10% increment until 60% concentration was reached. The result is depicted in Figure 10, showing that as Gamry's potentiostat tried to achieve the specific current ( $0.25 \text{ mA/cm}^2$ ), the potential increased until it achieved that value as a setting point for current. It can be seen from the figure that the increase in MEG concentration resulted in higher potential.

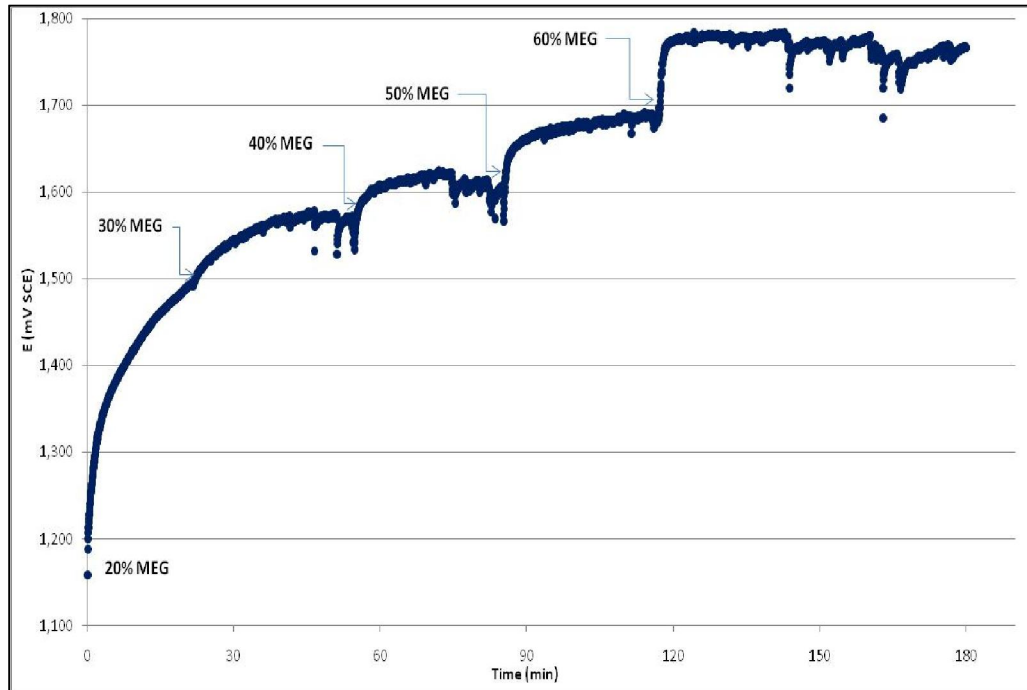


**Figure 10.** Potentials at  $0.25 \text{ mA/cm}^2$  applied current on Pt electrode, with 1 bar  $\text{CO}_2$  purged, 1% wt NaCl,  $40^\circ\text{C}$ , and 20-60% MEG addition

### 4.3 Rp/Ec Trend

#### 4.3.1 Corrosion Current

The corrosion resistance value measured from Rp/Ec scan was converted into corrosion current by using Tafel constants of 120 mV. From equation 26, corrosion resistance is inversely proportional to the corrosion current. Figure 11.a, c, and e show the plots of corrosion current for X-65 steel at  $20^\circ\text{C}$  with solution of various MEG and  $\text{HCO}_3^-$  concentration. MEG addition affected corrosion by reducing the corrosion current. In solution without MEG, final corrosion current varied between  $0.16 - 0.19 \text{ mA/cm}^2$ , in 25% MEG solution it reduces to  $0.07 - 0.12 \text{ mA/cm}^2$ , while in 50% MEG solution it decreased further to  $0.02 - 0.06 \text{ mA/cm}^2$ . Higher MEG will increase solution viscosity and decrease diffusivity,

and retard transfer of reactants for electrochemical reactions between bulk solution and steel surface. Decreased solution polarity due to MEG addition may also increase the solvation energy of the iron ions and decrease the activation and driving force for corrosion reaction [33].

Corrosion current of various series had different trend but relatively constant over time. Among all of the series with various  $\text{HCO}_3^-$  concentrations, series with 0 mmol/kg  $\text{HCO}_3^-$  had the highest corrosion current, while the lowest was series 15 mmol/kg  $\text{HCO}_3^-$ . Higher pH will normally reduce the corrosion rate and automatically, corrosion current, due to lack of  $\text{H}^+$  ions as reactants for cathodic reaction. As known before, in addition to  $\text{H}^+$  reduction, cathodic reaction is also dominated by  $\text{H}_2\text{CO}_3$  reduction at higher pH. With high  $\text{HCO}_3^-$  concentration, it was possible that the cathodic reaction rate increased and resulted in the increase of corrosion current as found by some previous authors [6]. Corrosion current differences between series 15 and 100 mmol/kg  $\text{HCO}_3^-$  that has average pH 6.2 and 7 respectively, was less than  $0.03 \text{ mA/cm}^2$ . This small deviation can be caused by steel surface variation.

Monitoring result for steel St-52 is shown in Figure 11.b, d, and f. Here, sampling frequency on some experiments was increased to give more data point. Effect of increase in MEG concentration was reduction on corrosion current. The final corrosion current in solution without MEG was between  $0.03 - 0.25 \text{ mA/cm}^2$ , which reduced to  $0.08 - 0.11 \text{ mA/cm}^2$  in 25% MEG solution, and  $0.035-0.06 \text{ mA/cm}^2$  in 50% MEG solution. In contrast to steel X-65, series 0 mmol/kg  $\text{HCO}_3^-$  with 0 and 25% MEG solutions had the lowest corrosion current. While series 15 mmol/kg  $\text{HCO}_3^-$  had the highest current. In solution without MEG, transport of reactants is not as hindered as solution with MEG, thus corrosion rate is supposed to be higher.

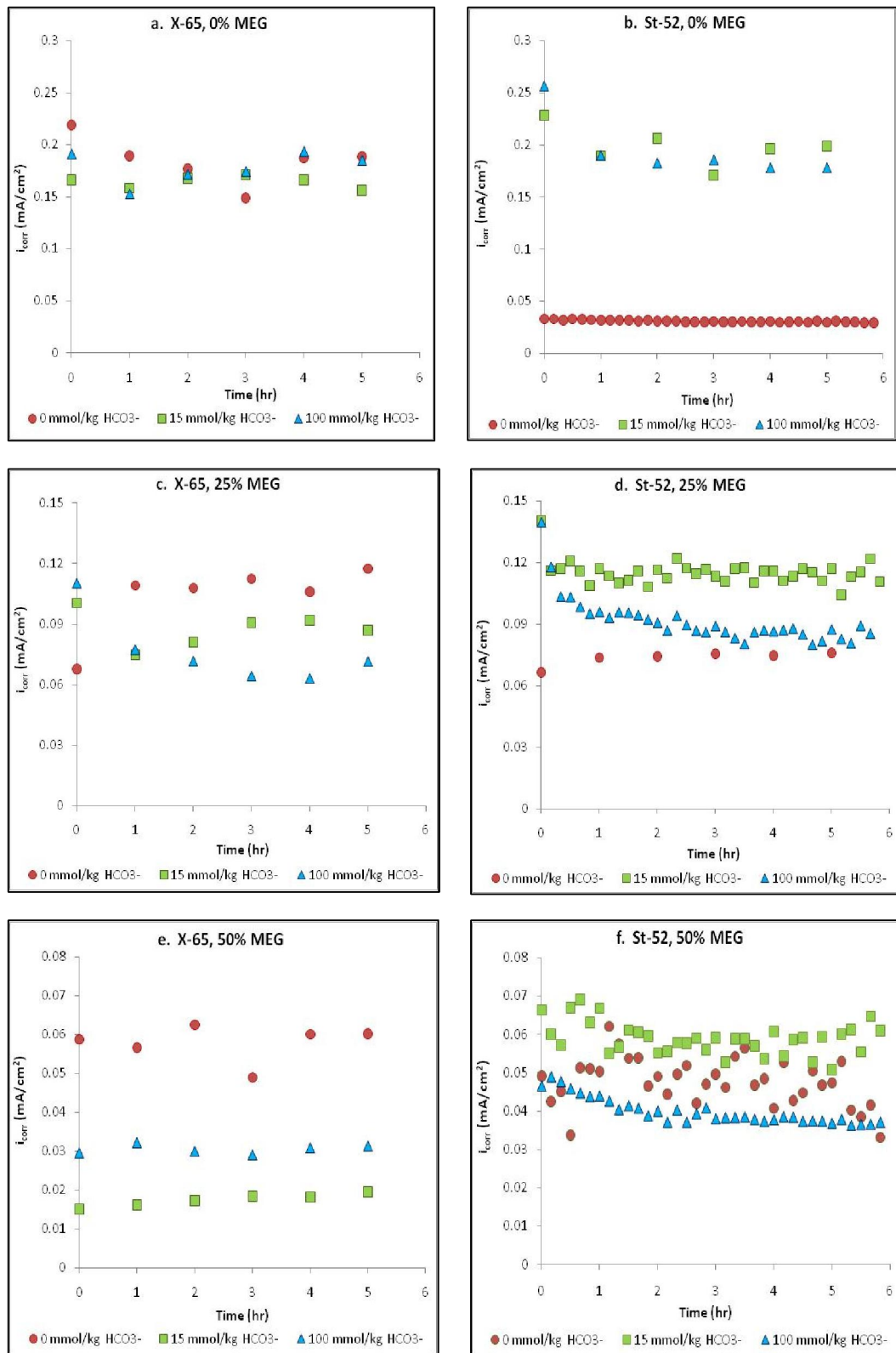


**Figure 11.** Corrosion current measurement on series 0-100 mmol/kg  $\text{HCO}_3^-$  at 20°C

These deviations of series 0 mmol/kg  $\text{HCO}_3^-$  which had the lowest corrosion rate at  $20^\circ\text{C}$  can be traced back to the previous experiment procedure, the potential measurement during pre-corrosion step (anodic galvanostatic). The anodic current applied also resulted in a far more positive voltage compared to other series (Figure 8.b). Since the deviation also occurred in the result, the potentiostat reliability during testing this series was questionable. Series 0 mmol/kg  $\text{HCO}_3^-$  was the last run in the whole experiment, and there was possibility that the accuracy of potentiostat had declined with time.

In 50% MEG solution (Figure 11.f), the corrosion currents of series 0 and 15 mmol/kg  $\text{HCO}_3^-$  oscillated within a limited value over time. In solution with lower  $\text{HCO}_3^-$  concentration, scaling tendency was low, and resulted in a formation of  $\text{FeCO}_3$  film with low degree of protectiveness. While at the same time, the removal of film occurred along with the film formation. These opposed processes lead to the fluctuation of current measurement with time. The experiment result also showed that effect of MEG at 50% concentration was obvious and it could hinder transport of  $\text{Fe}^{2+}$  away from steel surface. This condition was favorable for the formation of  $\text{FeCO}_3$  as  $\text{HCO}_3^-$  concentration was abundant in solution. The slow declining in corrosion current with time during 6 hours Rp/Ec scan is evidence that protective  $\text{FeCO}_3$  film was formed gradually.

Figure 12 illustrates the corrosion current from Rp/Ec measurement at  $40^\circ\text{C}$  for 6 hours. Results for steel X-65 are shown in Figure 12.a, c, e. The increase in MEG concentration affected the system by reducing the corrosion current. Final corrosion current for solution without MEG was  $0.27 - 0.32 \text{ mA/cm}^2$ , in 25% MEG solution was  $0.06 - 0.22 \text{ mA/cm}^2$ , while in 50% MEG was  $0.03 - 0.1 \text{ mA/cm}^2$ . Compared to experiment at  $20^\circ\text{C}$ , the corrosion current was slightly higher in this experiment. Reaction kinetic is enhanced by temperature, and since corrosion current is proportional to corrosion rate, it is clear that corrosion reaction is faster in higher temperature.

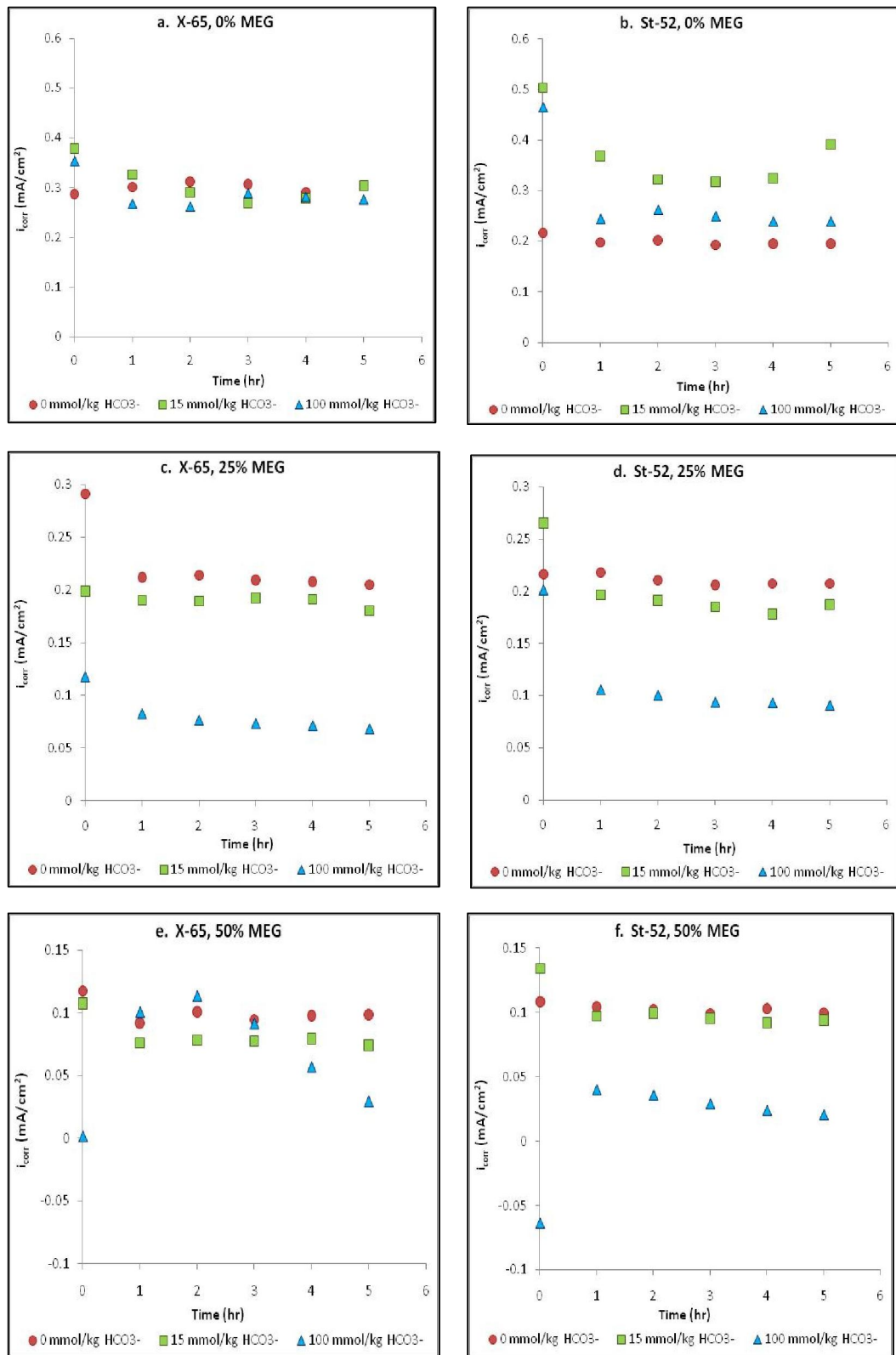


**Figure 12.** Corrosion current measurement on series 0-100 mmol/kg HCO<sub>3</sub><sup>-</sup>, at 40°C

There was similar trend among various MEG concentration (Figure 12.a, c, e), where the highest corrosion current was attained by series 0 mmol/kg  $\text{HCO}_3^-$ , and the lowest corrosion current was attained by series 100 mmol/kg  $\text{HCO}_3^-$ . In Figure 12.a, the corrosion current was relatively constant for series 0 mmol/kg  $\text{HCO}_3^-$ , while other series decreased first before approaching a steady value. The initial decrease in solution with  $\text{HCO}_3^-$  could be caused by adsorbed carbonate on the steel surface that was imposed by high pH and high temperature.

Series 100 mmol/kg  $\text{HCO}_3^-$  in 50% MEG solution behaved differently, in which it started at a very low, close to zero corrosion current. Pre-corrosion step (anodic galvanostatic) prior to  $R_p/E_c$  measurement showed how the series had a very high potential in the end of scans, indicating that there might be a protective  $\text{FeCO}_3$  film with passive layer formed on the steel surface. However, it then increased to  $0.12 \text{ mA/cm}^2$  after 2 hours allowed to corrode naturally without external applied current.  $\text{FeCO}_3$  film formation needs high supersaturation, thus as corrosion slowed down due to protective film formation,  $\text{Fe}^{2+}$  concentration would fall. While at the same time, there was film dissolution process occurred. This explains why corrosion increased first in a sudden, and then reduces gradually after there was enough  $\text{Fe}^{2+}$  for repairing  $\text{FeCO}_3$  film. It also indicated that  $\text{FeCO}_3$  film formed during pre-corrosion in the experiment condition ( $0.25 \text{ mA/cm}^2$  applied current, 24 hours) was not stable, and prone to dissolution. Nonetheless, corrosion current eventually dropped as system stabilized although the value was not as low as initial current.

Experiment result for St-52 is shown in Figure 12.b, d, and f. Addition of MEG had same result with the rest of experiment where it reduced the corrosion current. Compared to experiment at  $20^\circ\text{C}$  (Figure 11.b, d, and f), the corrosion current of St-52 was a little higher at  $40^\circ\text{C}$ . In solution without MEG the final current was  $0.2 - 0.4 \text{ mA/cm}^2$ , in 25% MEG solution it became  $0.09 - 0.21 \text{ mA/cm}^2$ , while in 50% MEG it was  $0.02 - 0.1 \text{ mA/cm}^2$ . However, at  $40^\circ\text{C}$ , more  $\text{FeCO}_3$  film was expected to form than at lower temperature since the solubility decreased with

temperature increase. It can also be seen that series 100 mmol/kg  $\text{HCO}_3^-$  in 50% MEG has the lowest corrosion current among all.

In solution without MEG (Figure 12.b), series 0 mmol/kg  $\text{HCO}_3^-$  had the lowest corrosion current, while series 15 mmol/kg  $\text{HCO}_3^-$  has the highest corrosion current. This was similar to the experiment at 20°C but the deviation was not as extreme as experiment at 20°C. Series 100 mmol/kg  $\text{HCO}_3^-$  had its corrosion current decreased with time, since  $\text{FeCO}_3$  formation needs more time without MEG. The surprisingly low corrosion current of series 0 mmol/kg  $\text{HCO}_3^-$  might be caused by steel surface modification during anodic galvanostatic step, which shows steep increase in potential with time (Figure 9.b). Moreover, the absence of MEG that could hinder transport of reactants resulted in less marked effect of  $\text{HCO}_3^-$  addition. However, it is recommended that this experiment was repeated to confirm the low corrosion rate.

Figure 12.d and f that show experiment in 25% and 50% MEG, had corrosion current which reduced as  $\text{HCO}_3^-$  concentration increased. MEG that was present in the solution increased the viscosity and decreased diffusivity, hindering ions transfer. Thus, the effect of  $\text{HCO}_3^-$  addition, as one of main ions taking important part in corrosion reactions was more observable here.

Series 0 mmol/kg  $\text{HCO}_3^-$  in various MEG concentrations (Figure 12.b, d, and f) had relatively constant corrosion currents over time, meaning that there was almost no modification in the overall corrosion film. Corrosion current of series 15 mmol/kg  $\text{HCO}_3^-$  initially dropped, then decreased slowly with time. This trend was also shown by series 100 mmol/kg  $\text{HCO}_3^-$  in Figure 12. b and d, showing that  $\text{FeCO}_3$  formation was initially high in the start of scanning period due to exposure of carbide and high  $\text{Fe}^{2+}$  after pre-corrosion step. Since the steel was not forced to corrode by external anodic current, and available  $\text{Fe}^{2+}$  was consumed by formation of  $\text{FeCO}_3$ , the corrosion current became lower.

Corrosion current behavior of series 100 mmol/kg  $\text{HCO}_3^-$  in 50% MEG can be seen in Figure 12.f. The phenomenon was similar to steel X-65 with slightly lower

current value. The potential increased first then decreased with time showing partial dissolution of iron carbonate film. Some authors also suggested that iron carbonate film formation at temperature less than 60°C will need higher supersaturation and easily dissolves back to the solution leaving a porous structure [6, 36].

In general corrosion current in steel X-65 was lower compared to steel St-52. Higher carbide phase that could potentially be formed in St-52 might result in galvanic coupling and local acidification leading to higher corrosion rate. High  $\text{HCO}_3^-$  additions would increase the solution pH and supersaturation for  $\text{FeCO}_3$  formation. Thus, in condition where protective  $\text{FeCO}_3$  formation was favorable, corrosion current in St-52 will be lower than X-65.

#### **4.3.2 Corrosion Potential**

Corrosion potential shown in Figure 13 and 14 is a result of 6 hours Rp/EC trend measurement at 20°C and 40°C respectively. For experiment at 20°C, the potential measured on steel X-65 was similar to steel St-52. Addition of MEG in X-65 (Figure 13.a, c, e) did not have marked effect on the corrosion potential. The final potential in solution without MEG was -640 to -688 mV, in 25% MEG solution was -635 to -695 mV, and in 50% MEG solution was -611 to -688 mV. From those three different MEG concentrations, all had common trend, in which potential shifted to more negative value as  $\text{HCO}_3^-$  concentration increased. All of the curves decreased with time towards steady state. Some experiments performed by other authors mentioned corrosion potential -710 mV to -630 mV (vs AgCl) when they increased MEG concentration from 0% to 70% at X-65 under condition of 25°C, 1 bar  $\text{CO}_2$ , pH 5, 10g/L NaCl and natural convection [33].

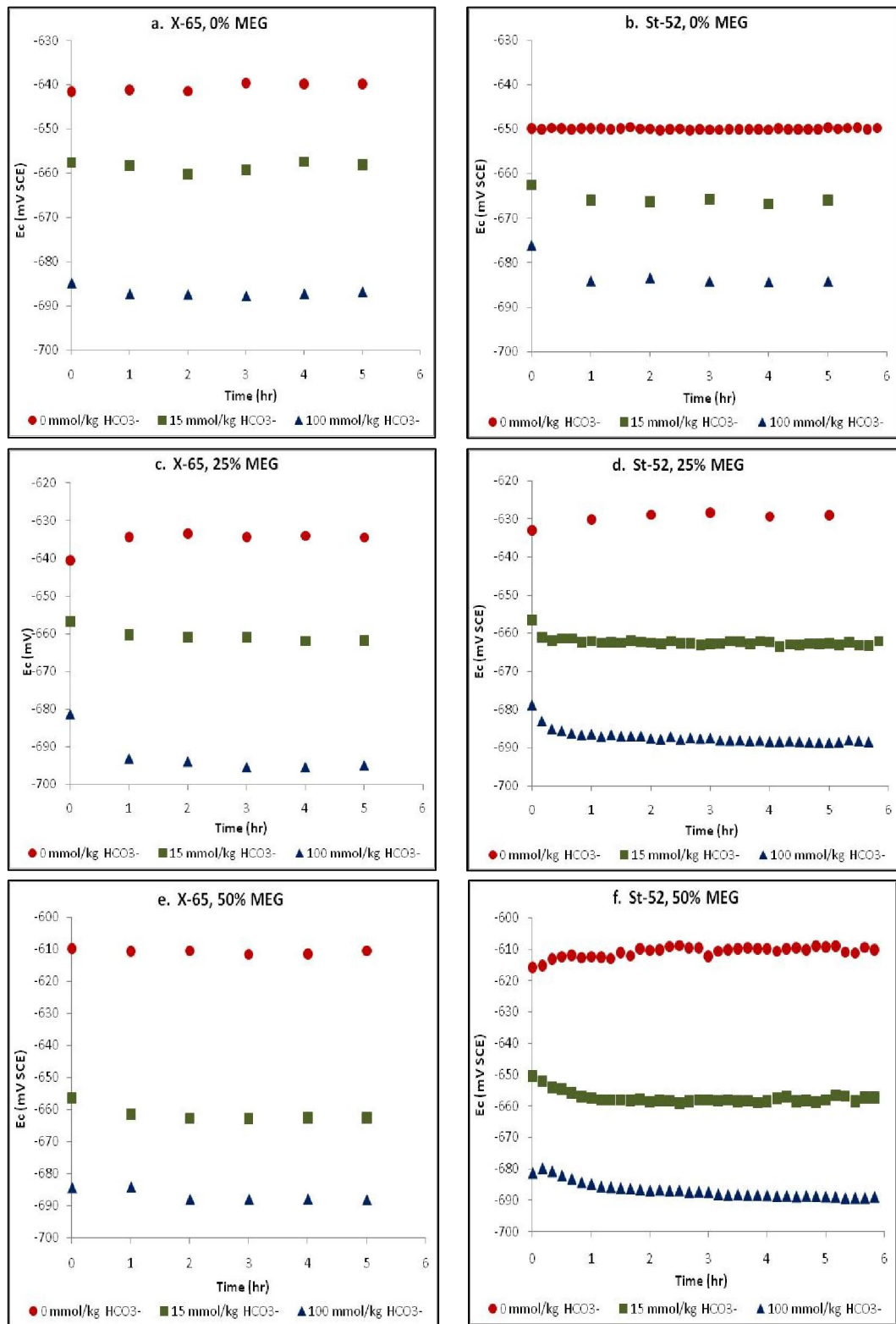


**Figure 13.** Corrosion potential measurement on series 0-100 mmol/kg  $\text{HCO}_3^-$ , at 20°C

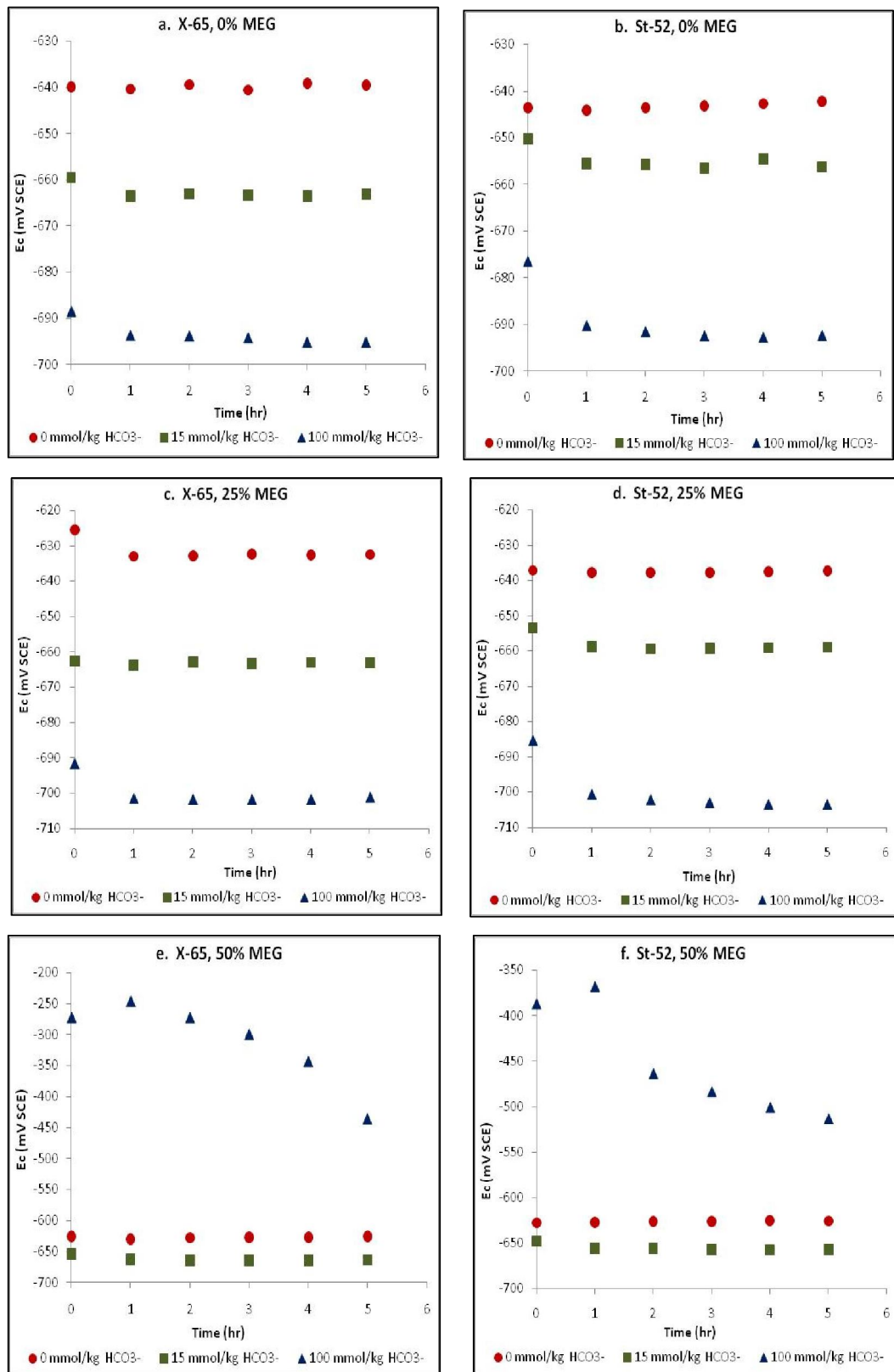


**Figure 14.** Corrosion potential measurement on series 0-100 mmol/kg  $\text{HCO}_3^-$ , at 40°C

Figure 13.b, d, and f illustrate the potential measurement in St-52 at 20°C. Solution without MEG had potential between -650 mV to -684 mV, solution with 25% MEG between -629 mV to -688 mV, and potential in solution with 50% MEG varied between -610 mV to -689 mV. Similar to X-65, HCO<sub>3</sub><sup>-</sup> increase in various MEG concentration resulted in more negative potential. The potentials had small decrease in the start of scanning and stabilized to a steady value, except for series 0 mmol/kg HCO<sub>3</sub><sup>-</sup> which was relatively stable over time.

Experiment result of steel X-65 conducted at 40°C (Figure 14.a, c, and e), resulted in final potential for solution without MEG between -639 mV to -695 mV, for 25% MEG solution between -638 mV to -700 mV, and for 50% MEG solution between -435 mV to -663 mV. Steel St-52 results are shown in Figure 14.b, d, and f. The final potential of St-52 in various MEG concentrations was in the same range with X-65. In solution without MEG, the value was between -642 mV to -692 mV, in 25% MEG solution was between -637 mV to -703 mV, while in 50% MEG solution the value ranged between -513 mV to -657 mV.

For both steels, the increase in MEG concentration did not have clear trend, as also found in experiment at 20°C. In solution without MEG and with 25% MEG, the addition of HCO<sub>3</sub><sup>-</sup> caused a more negative potential. This tendency was also occurred in experiment at 20°C. Comparing experiment result at 20°C (Figure 13) to experiment at 40°C (Figure 14), it can be seen that the value was similar. The only marked difference was on the series 100 mmol/kg HCO<sub>3</sub><sup>-</sup> in 50% MEG. From evidence that potential declined with the addition of HCO<sub>3</sub><sup>-</sup> while the effect on current was not significant, it can be hypothesized that most likely only either cathodic or anodic reaction was highly affected.

The high potential in series 100 mmol/kg HCO<sub>3</sub><sup>-</sup> of both steels (Figure 14.e and f) was suspected to be caused by protective FeCO<sub>3</sub> formation as predicted in anodic galvanostatic result (Figure 9.e and f) and low corrosion current measured (Figure 12.e and f). With high HCO<sub>3</sub><sup>-</sup> concentration, it seemed that FeCO<sub>3</sub> film formed on

the steel surface was thick enough to create a barrier and retard electrochemical reactions.

In addition, high MEG concentration made the retardation effect due to corrosion film presence even worse. The reduction of anodic and cathodic reactions part in this series could shift the corrosion potential to a more positive value. This showed by the series behavior which started at a very high potential, followed by a little increase, and then decreased with time to a value which was lower than the initial potential. The declining tendency in the later measurement period was possibly due to the dissolution of some  $\text{FeCO}_3$  film as the corrosion was allowed to proceed naturally. This trend in potential was consistent with the trend in corrosion current. The steel surface seemed to be modified by the applied anodic current during pre-corrosion step (galvanostatic), which resulted in a very positive potential at the beginning of measurement. After the disturbance current was removed, there was less  $\text{Fe}^{2+}$  leading to lower supersaturation, and the potential decreased with time.

#### **4.4 Iron Concentration Analysis**

Iron concentration in solution was measured twice, before and after the Rp/Ep scan. Prior to Rp/Ep scan, procedure that was performed on the cell consisted of measurement of open corrosion potential, cathodic potentiodynamic, anodic galvanostatic, and cathodic potentiodynamic.

To find out if iron carbonate could form on the steel surface, a simple manual calculation was performed to obtain the iron concentration needed to achieve  $\text{FeCO}_3$  saturation. The relevant reactions from Chapter 2 are summarized in Table 5, while equations to calculate the equilibrium constants are listed in Table 6. It was assumed that an equilibrium condition was attained, and ionic strength contribution was omitted to simplify the equations. By combining equilibrium

constant in Table 5, concentration of  $CO_3^{2-}$  was calculated based on solution pH and  $CO_2$  pressure data.

**Table 5.** Chemical reactions and the equilibrium constant [1]

	Reaction	Equilibrium Constant
Dissolution of carbon dioxide	$CO_2(g) \rightleftharpoons CO_2(aq)$	$K_{sol} = \frac{c_{CO_2}}{p_{CO_2}}$
Water dissociation	$H_2O \rightleftharpoons H^+ + OH^-$	$K_{wa} = c_{H^+} \cdot c_{OH^-}$
Carbon dioxide hydration	$CO_2(g) + H_2O \rightleftharpoons H_2CO_3$	$K_{hy} = \frac{c_{H_2CO_3}}{c_{CO_2}}$
Carbonic acid dissociation	$H_2CO_3 \rightleftharpoons H^+ + HCO_3^-$	$K_{ca} = \frac{c_{H^+} \cdot c_{HCO_3^-}}{c_{H_2CO_3}}$
Bicarbonate anion dissociation	$HCO_3^- \rightleftharpoons H^+ + CO_3^{2-}$	$K_{bi} = \frac{c_{H^+} \cdot c_{CO_3^{2-}}}{c_{HCO_3^-}}$
Iron carbonate precipitation	$Fe^{2+} + CO_3^{2-} \rightarrow FeCO_3$	$K_{wa} = c_{Fe^{2+}} \cdot c_{CO_3^{2-}}$

**Table 6.** Formula to calculate equilibrium constant for reactions in Table 5 [1]

$K_{sol} = \frac{14.5}{1.00258} \times 10^{-(2.27+5.65 \times 10^{-3} T_f - 8.06 \times 10^{-6} T_f^2 + 0.075 \times I)}$
$K_{wa} = 10^{-(29.3868 - 0.0737549 \times T_k + 7.47881 \times 10^{-5} T_k^2)}$
$K_{hy} = 2.58 \times 10^{-3}$
$K_{ca} = 387.6 \times 10^{-(6.41-1.549 \times 10^{-3} T_f + 8.52 \times 10^{-6} T_f^2 - 3.07 \times 10^{-5} p - 0.4772 \times I^{0.5} + 0.118 \times I)}$
$K_{bi} = 10^{-(10.61 - 4.97 \times 10^{-3} \times T_f + 1.331 \times 10^{-5} T_f^2 - 2.624 \times 10^{-5} p - 1.166 \times I^{0.5} + 0.3466 \times I)}$

Note:  $T_f$  is temperature in degree Fahrenheit,  $T_k$  is temperature in Kelvin,  $I$  is ionic strength in molar, and  $p$  is the pressure in psi.

Solubility products of  $FeCO_3$  was calculated using Equation 20, which resulted in  $pK_{sp}$  of 10.86 at 20°C and 10.99 at 40°C. Apart from simplification in the calculation, this value was used as rough estimation since it was close to the literature value; 10.54 at 25°C [25, 36]. The minimum iron concentration required to achieve  $FeCO_3$  saturation can be obtained by dividing solubility product with carbonate ion concentration. Calculation result is summarized in Table 7.

**Table 7.** Estimated iron concentration required for saturation

Solution pH	$HCO_3^-$ addition (mmol/kg)	Required $Fe^{2+}$ (ppm)	
		20°C	40°C
4	0	10307.806	8772.448
6.2	15	0.410	0.349
7	100	0.010	0.009

From the calculation result in Table 7, it can be seen that at pH 4 (0 mmol/kg  $HCO_3^-$  addition),  $Fe^{2+}$  concentration needed to exceed  $K_{sp}$  of  $FeCO_3$  had to be more than 10000 ppm. Without addition of external  $Fe^{2+}$ , such high iron concentration was impossible to obtain in normal steel corrosion under  $CO_2$

environment. There was low possibility of  $\text{FeCO}_3$  formation in this low pH condition. On the other hand, as pH was increased to 6.2 by addition of 15 mmol/kg  $\text{HCO}_3^-$ , the required  $\text{Fe}^{2+}$  concentration dropped to 0.41 ppm. These findings eliminate possibility of  $\text{FeCO}_3$  formation as the cause of low corrosion current in series 0 mmol/kg  $\text{HCO}_3^-$  at 20°C as found in experiment with St-52 (Figure 11.a). This result also strengthens the hypothesis that the Gamry potentiostat accuracy declined with its running hour. Thus for the last experiment which was series 0 mmol/kg  $\text{HCO}_3^-$  of St-52 at 20°C, the electrochemical testing result was not reliable anymore.

Nonetheless, it should be bear in mind that this was concentration in bulk solution, which did not necessarily represent concentration near steel surface. Limited formation of  $\text{FeCO}_3$  on steel surface with low degree of protectiveness is still possible to occur, especially with high  $\text{Fe}^{2+}$  concentration trapped between the carbide structures. While in higher pH, as the iron concentrations exceed the saturation concentration, the formation of  $\text{FeCO}_3$  was expected to occur in a more massive manner due to high supersaturation. As supersaturation of  $\text{FeCO}_3$  become higher, the possibility of protective film to be found will increase with a better level of protectiveness. Experiments done by Berntsen et.al showed that required supersaturation to form a protective  $\text{FeCO}_3$  film in 1 bar  $\text{CO}_2$ , 1%wt NaCl, 50% MEG at 20°C was approximately 300 [37].

Iron analysis result for both X-65 and St-52 is summarized in Table 8. Effect of MEG addition in X-65 was a reduction in iron concentration, while in St-52 there was no clear trend that can be observed. Temperature seemed to increase the iron concentration in solution with X-65, since it enhanced the kinetic of corrosion. However, some exceptions are in solution of 0 mmol/kg  $\text{HCO}_3^-$  with 0% and 50% MEG, and in the solution of 100 mmol/kg  $\text{HCO}_3^-$  with 50% MEG. In 0 mmol/kg  $\text{HCO}_3^-$  solution, pH was acidic and  $\text{FeCO}_3$  was not able to form. So the first case was most likely caused by error in measurement. While in the second case, solution pH in 100 mmol/kg  $\text{HCO}_3^-$  was high, combined with high temperature, creating a condition which was favorable for  $\text{FeCO}_3$  formation. The film

formation would consume iron ions, and consequently the concentration in bulk solution at 40°C was lower than at 20°C.

**Table 8.** Iron analysis result

No	T (°C)	MEG (%wt)	HCO <sub>3</sub> <sup>-</sup> (mmol/kg)	X-65		St-52	
				Fe <sup>2+</sup> before Rp/Ec Scan (ppm)	Fe <sup>2+</sup> after Rp/Ec Scan (ppm)	Fe <sup>2+</sup> before Rp/Ec Scan (ppm)	Fe <sup>2+</sup> after Rp/Ec Scan (ppm)
1	20	0	0	10.4	12.5	99.7	7.7
2			15	3.0	4.0	37.7	7.0
3			100	2.2	2.7	4.0	4.0
4		25	0	7.4	8.1	5.4	6.7
5			15	3.3	4.9	5.0	6.7
6			100	1.4	3.1	2.9	2.9
7		50	0	4.7	6.8	3.4	3.2
8			15	3.1	1.1	23.6	3.7
9			100	3.8	2.5	4.2	3.0
10	40	0	0	9.0	10.1	14.5	13.9
11			15	6.9	7.2	7.1	7.4
12			100	2.7	2.2	2.5	2.3
13		25	0	7.9	9.1	7.4	8.4
14			15	5.7	5.9	5.0	5.5
15			100	3.5	3.3	2.7	2.8
16		50	0	4.5	5.3	5.2	5.5
17			15	3.5	4.3	4.5	3.9
18			100	2.1	1.9	5.9	1.9

In steel X-65, the increase of HCO<sub>3</sub><sup>-</sup> concentration added into solution was followed by the decreased of iron concentration measured. Regarding to the time of measurement (between before and after Rp/Ec scan), there were variations in the result. The iron concentration increased in all solution without HCO<sub>3</sub><sup>-</sup>. This shows that as corrosion progress, there was no or limited FeCO<sub>3</sub> formation that might consume iron ions and reduce the concentration in solution. This finding proves the previous hypothesis that FeCO<sub>3</sub> formation was not expected to occur at series 0 mmol/kg HCO<sub>3</sub><sup>-</sup>, or pH 4.

In series 15 mmol/kg  $\text{HCO}_3^-$ , the concentration decreased only in 50% MEG solution at 20°C, while in other case it increased. This result was confirmed with corrosion current measurement (Figure 11.e) which was low, indicating that corrosion was retarded, possibly by protective film. The same condition was also found in 100 mmol/kg  $\text{HCO}_3^-$ , where  $\text{FeCO}_3$  formation was expected to take place due to high pH. So, it is obvious that main cause for  $\text{Fe}^{2+}$  reduction between two iron concentration measurements was  $\text{FeCO}_3$  formation.

Effect of temperature in St-52 was unclear, even though most of them showing increased value with the increase of temperature. While the effect of  $\text{HCO}_3^-$  addition is the decrease in  $\text{Fe}^{2+}$  concentration. The two main reasons for the decrease in iron concentration were lower corrosion rate producing less  $\text{Fe}^{2+}$ , and the high pH that might lead to  $\text{FeCO}_3$  formation depleting the available  $\text{Fe}^{2+}$ .

Other interesting fact was that in many of experiment with St-52,  $\text{Fe}^{2+}$  concentration before Rp/Ec scan was higher than after the scan. This could be caused by  $\text{FeCO}_3$  formation which developed during the time between two measurements, such as in condition where the process was favorable (high  $\text{HCO}_3^-$  and MEG concentration). The iron carbonate formation process consumed  $\text{Fe}^{2+}$  so that the concentration diminished with time. Meanwhile, in series 0 and 15 mmol/kg  $\text{HCO}_3^-$  with 0% MEG solution,  $\text{FeCO}_3$  formation was expected to be limited. However,  $\text{Fe}^{2+}$  concentration was very high during the first measurement. It was possibly because of the high corrosion rate during anodic galvanostatic producing high  $\text{Fe}^{2+}$  concentration in bulk solution. The elevated  $\text{Fe}^{2+}$  concentration facilitated supersaturation of  $\text{FeCO}_3$  for series 15 mmol/kg  $\text{HCO}_3^-$ . In addition, exposure of carbide phase in St-52 during pre-corrosion (anodic galvanostatic), provided anchor for  $\text{FeCO}_3$  film. These facts suggest that  $\text{FeCO}_3$  with some degree of protection was possible to be formed. Corrosion current measurement (Figure 11.d) also showed a relatively low corrosion rate that confirmed the result.

There were some error sources that might cause variations in  $\text{Fe}^{2+}$  measurements. Sample for  $\text{Fe}^{2+}$  analysis was taken from certain point in bulk solution, while in the cell there was no stirring device and the solution circulation was based on natural convection. Basically, there was no means to ensure that concentration in all point of solution was identical at certain time. Other possible source was oxygen intrusion into the cell. This could happen as the solution was exposed to air during sampling. The sampling was done manually by opening stopper to insert a pipette for less than 5 seconds, and then sealed it back afterwards. In spite of short exposure time, series 0 and 15 mmol/kg  $\text{HCO}_3^-$  in 0% MEG solution at  $20^\circ\text{C}$  turned slightly yellow in the end of experiment using steel St-52. This indicates that  $\text{Fe}^{2+}$  is oxidized by oxygen, resulting in  $\text{Fe}^{3+}$ , which could be in the form of amorphous  $\text{Fe}(\text{OH})_3$  and  $\alpha\text{-FeOOH}$  which has yellow color [38]. Kvarekval et.al. also found that addition of oxygen to a  $\text{CO}_2$  active corrosion with pH stabilization could enhance the formation of protective  $\text{FeCO}_3$  film [38]. The introduction of oxygen in the middle of their experiment caused a decrease in the corrosion rate. The same phenomenon occurred in this case with low or no  $\text{HCO}_3^-$  addition and no MEG solution, where corrosion current measurement done after the first iron measurement showed a very low value (Figure 11.b and d).

#### **4.5 Potentiodynamic Scans**

Potentiodynamic scans were done as the last electrochemical testing procedure in the experiment. The cathodic sweep was done first, and then the system was allowed to stabilize for 10 minutes before starting anodic sweep. Both of the potentiodynamic scan were started -5 mV or +5 mV from open corrosion potential, respectively for the anodic and cathodic sweeps. Result for X-65 at  $20^\circ\text{C}$  is shown in Figure 15.a, c, and e. The increase in MEG concentration resulted in the shift of open corrosion potential to a slightly more positive value, while at the same time moving the corrosion current to the lower value.

Gulbrandsen found the similar phenomenon and suggested that the decreased in the corrosion current was due to the decrease in  $\text{CO}_2$  solubility, water activity, and  $\text{H}_2\text{CO}_3$  diffusivity due to increasing solution viscosity [33]. Regarding to the potentiodynamic curve shape, it can be seen that anodic part did not change. On the other hand, the cathodic part was slightly altered especially in series with  $\text{HCO}_3^-$  addition.

The addition of  $\text{HCO}_3^-$  showed less marked effect on the shape of anodic curve in the three different MEG concentrations. Nesic et.al. also found that pH has small effect on the anodic dissolution reaction of iron [3]. On the other hand, pH had an obvious change in the cathodic curve. As can be seen in experiment without MEG (Figure 15.a), solution without  $\text{HCO}_3^-$  addition had a distinct limiting current. While in 15 mmol/kg  $\text{HCO}_3^-$  solution, portion of curve which exhibited limiting current was reduced. By the increase of  $\text{HCO}_3^-$  concentration (pH increased from 4 to 6.2), the limiting current was not clearly seen. Similar trend was also found in experiment with 25% MEG and 50% MEG solution. The indistinguishable limiting current demonstrated that as pH increased, cathodic reaction was not only dominated by  $\text{H}^+$  reduction, but also by  $\text{H}_2\text{CO}_3$  reduction. Limiting current in  $\text{CO}_2$  corrosion is a caused by depletion of  $\text{H}^+$  ions on the steel surface and slow hydration of  $\text{CO}_2$  [1].

With the increase of  $\text{HCO}_3^-$  concentration, it can be seen that cathodic curve is slanted at low potential. This behavior was caused by the reduction of  $\text{H}_2\text{O}$  which was also found by Nesic at.al. [3]. Series 100 mmol/kg  $\text{HCO}_3^-$  was the most sensitive to the addition of MEG. By comparing cathodic part of the series in various MEG concentration (Figure 15.a, c, and e), it is clear that the angle of inflection is greater as MEG concentration is increased while the limiting current part in cathodic sweep was reduced. This shows that at higher MEG concentration and high pH, water reduction dominates cathodic reaction. Reduction of  $\text{H}_2\text{CO}_3$  and  $\text{H}^+$  were less pronounced because those reactions are mass transfer controlled which were retarded as a consequent of high viscosity and low diffusivity in MEG solution.

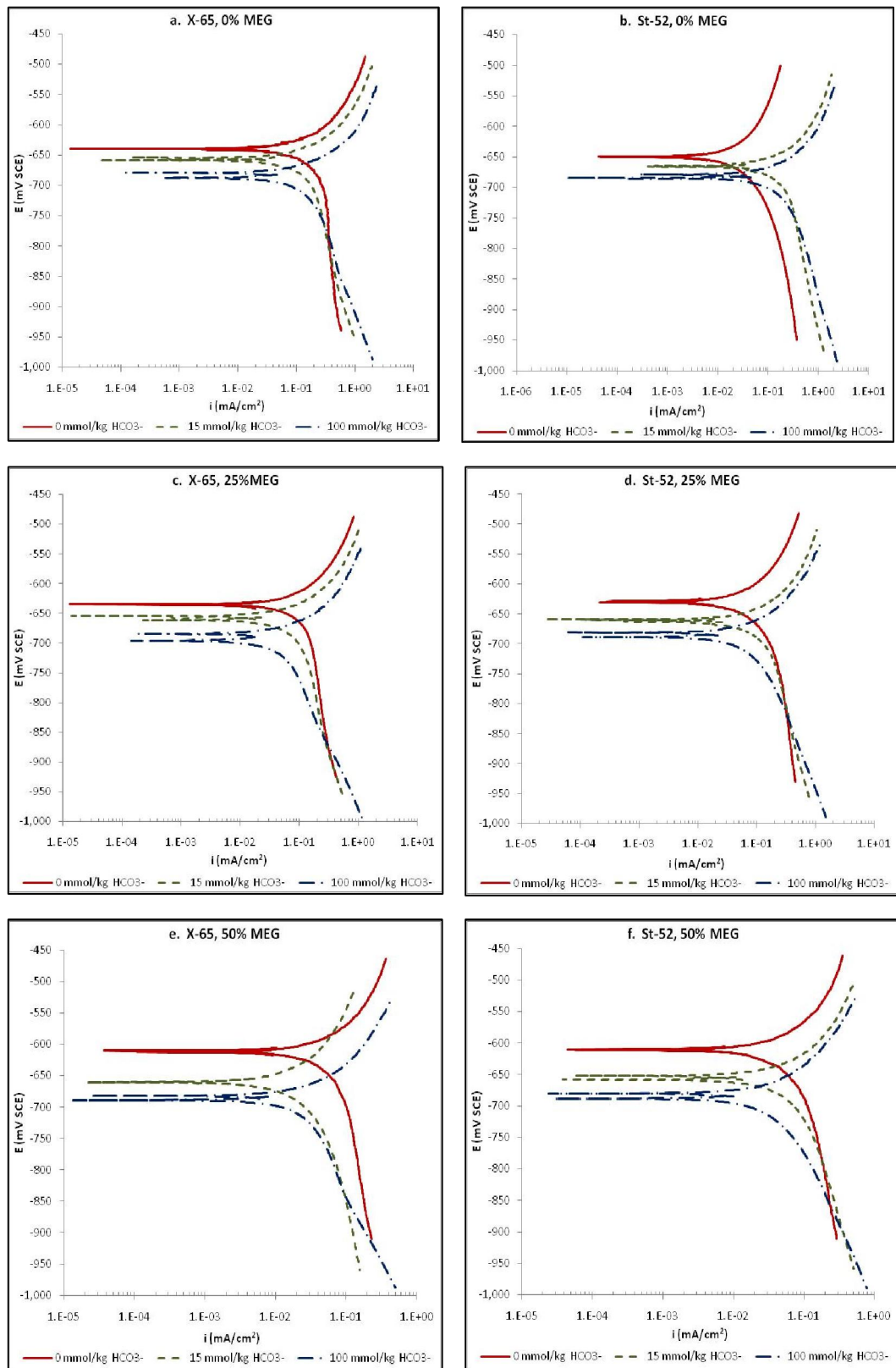


**Figure 15.** Potentiodynamic sweep on series 0-100 mmol/kg HCO<sub>3</sub><sup>-</sup>, at 20°C

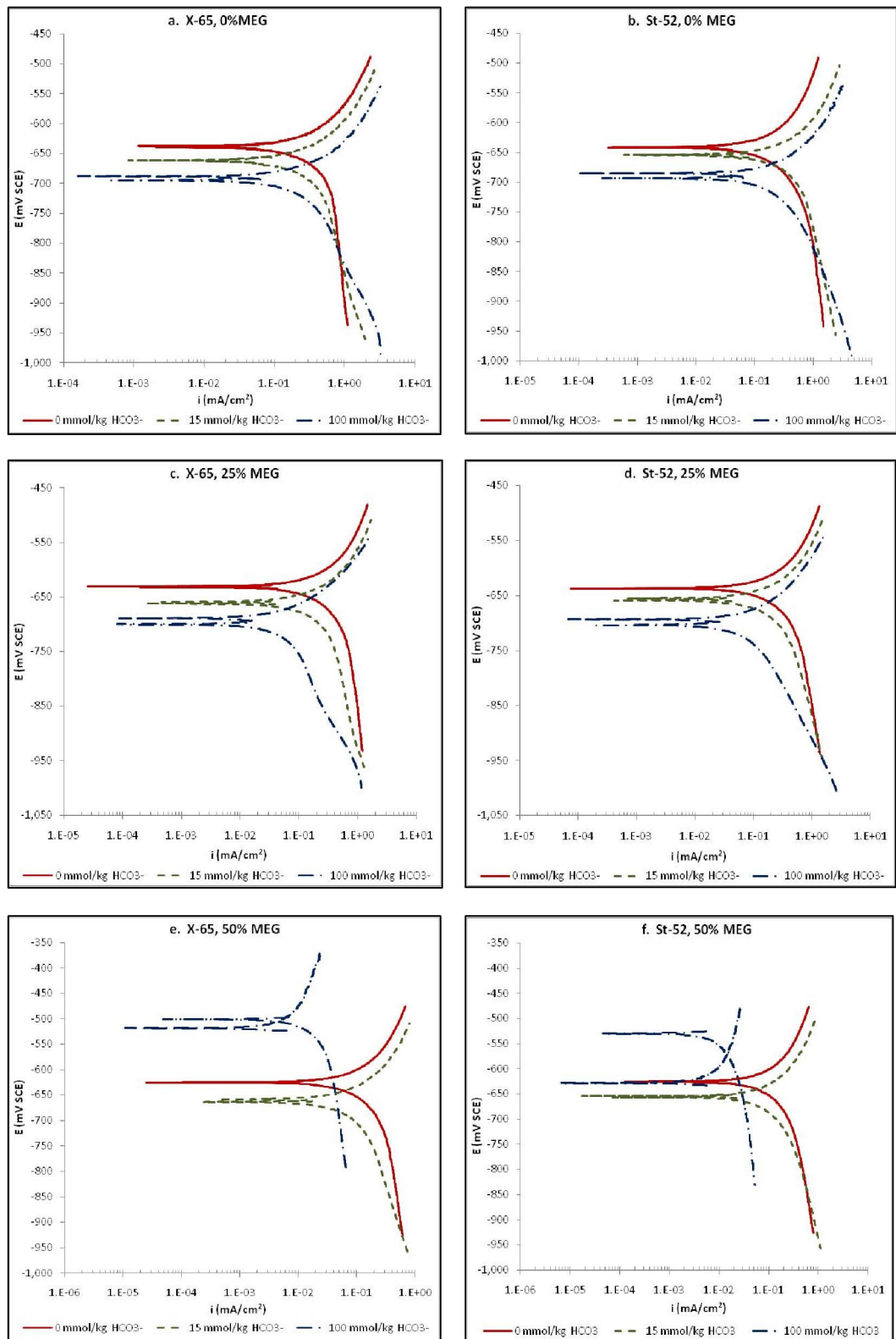


**Figure 16.** Potentiodynamic sweep on series 0-100 mmol/kg HCO<sub>3</sub><sup>-</sup>, at 40°C

Experiment result for steel St-52 at 20°C is shown in Figure 15.b, d, and f. Effect of MEG addition was the small shift of corrosion potential to a more positive direction, and reduction of the corrosion current. The addition of  $\text{HCO}_3^-$  was followed by reduction in corrosion current and corrosion potential. These findings on St-52 are similar to X-65. However, series 0 mmol/kg  $\text{HCO}_3^-$  in solution with 0% MEG and 25% MEG showed deviation from the trend. Those series had the lowest corrosion current compared to other series that contain  $\text{HCO}_3^-$ . The same deviations on series 0 mmol/kg  $\text{HCO}_3^-$  were also found in the anodic galvanostatic,  $R_p/E_c$  measurement, and iron concentration measurement. These findings confirm the possibility of a decline in Gamry's accuracy as explained previously.

The shape of anodic part in potentiodynamic curve of St-52 did not affected by MEG and  $\text{HCO}_3^-$  addition, similar to X-65. While the cathodic part of the curve changed a little as MEG and  $\text{HCO}_3^-$  concentration increased. The increase in  $\text{HCO}_3^-$  concentration was followed by the disappearance of limiting current. Exception was for series 0 mmol/kg  $\text{HCO}_3^-$  which had deviation as previous testing result. Similar to X-65, with the increase of  $\text{HCO}_3^-$ , the inflection of cathodic curve at low potential became apparent. As the pH increased due to  $\text{HCO}_3^-$  addition, the cathodic reaction seemed to be charge transfer controlled rather than mass transfer controlled. However, MEG addition did not show observable effect on the shape of cathodic curve. St-52 in general attained slightly higher cathodic current compared to X-65. This was caused by higher carbon content in St-52 that might form carbide phase during pre-corrosion step.

Result for potentiodynamic sweep at 40°C was depicted in Figure 16. In both X-65 and St-52, the open corrosion potentials were close to the value from experiment at 20°C. The limiting current was higher at 40°C, consistent with the  $R_p/E_c$  measurement. The obvious difference from experiment at 20°C was the cathodic curve shape of series 100 mmol/kg  $\text{HCO}_3^-$ . It can be seen from Figure 16.a and c for steel X-65, that the cathodic curve had indistinct indication of water

reduction. Meanwhile, in steel St-52 (Figure 16.b and d), the effect of temperature increment was less pronounced.

In Figure 16.e and f, series 100 mmol/kg  $\text{HCO}_3^-$  showed different behavior compared to the rest of experiment. For both steels, the cathodic curve overlapped with anodic curve. The series also had a very positive corrosion potential and very low corrosion current density. The lag time between cathodic and anodic for system to stabilize was constant for all experiment. However, the series indicated that there was disturbance that hindered the system to reach the open corrosion potential back after cathodic potentiodynamic polarization within designated time. The result from previous testing procedure pointed out that in this series, there was  $\text{FeCO}_3$  film and passive layer formed.  $\text{FeCO}_3$  film that formed on the steel surface was the major resistance for the system to go back into its initial open corrosion potential after being polarized cathodically. Figure 16.f for St-52 showed larger difference between the starting points for each scan, i.e the open corrosion potential. This could be a sign for  $\text{FeCO}_3$  film thickness that acted as system resistance.

Higher  $\text{FeCO}_3$  formation on St-52 was the direct consequence of more carbide formed on the type of steel. Some pictures of sample after the experiments are shown in Figure 17 in order to compare corrosion process underwent by St-52. Figure 17.a depicted sample from series 100 mmol/kg  $\text{HCO}_3^-$ , 50% MEG at 40°C. While Figure 17.b was a sample from series 0 mmol/kg  $\text{HCO}_3^-$ , 0% MEG at 20°C, which showed abnormality in the electrochemical testing result. It is clear from Figure 17.a that localized corrosion occurred with some visible white layer on the sample surface that was indicated as  $\text{FeCO}_3$ . The localized corrosion resembled pitting type which shows wormhole pattern attack and interconnected in some part. On the other hand, from Figure 17.b it can be seen that under the experiment condition, the steel got uniform corrosion, and no visible film of  $\text{FeCO}_3$ . Thus, the low corrosion rate measured was misleading and confirmed the inaccuracy of Gamry potentiostat.

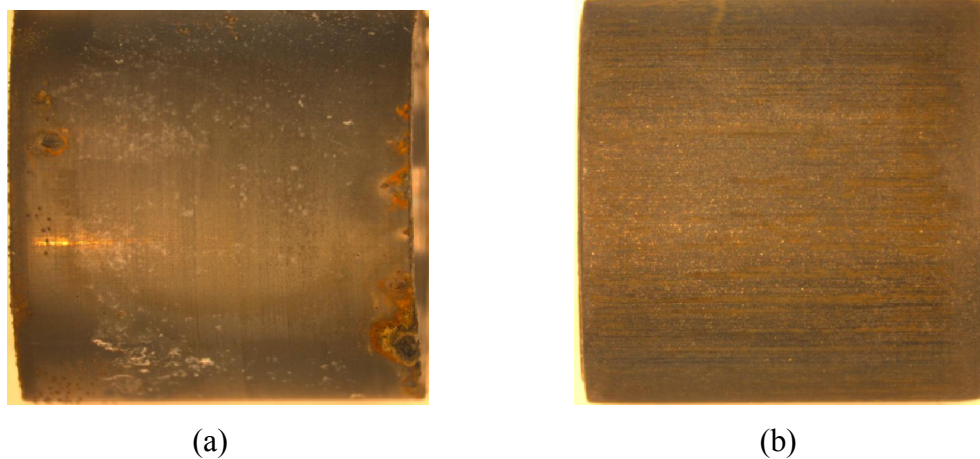


**Figure 17.** Sample surface after experiment (a. Series 100 mmol/kg  $\text{HCO}_3^-$ , 50% MEG at 40°C; b. Series 0 mmol/kg  $\text{HCO}_3^-$ , 0% MEG at 20°C)

The weight loss measurement is attached in Appendix D, but the result was used only to check the corrosion testing result. In general, the increase in  $\text{HCO}_3^-$  and MEG concentration was followed by the increase in weight loss. Only some shows a constant value, which can be caused by the small sample size and weight loss that could be measured, all of which leading to error in measurement. Sample St-52 in series 100 mmol/kg  $\text{HCO}_3^-$ , 50% MEG at 40°C gain small weight (0.08%) after the experiment. This finding strengthens the hypothesis that  $\text{FeCO}_3$  formed on the steel surface during experiment of that series.

Unfortunately, SEM analysis on the experiment result was not conducted due to time limitation. SEM image on X-65 steel on experiment that was done by Laethaisong is shown in Figure 18 as an illustration. EDS (Energy Dispersed X-Ray) analysis revealed that there were  $\text{FeCO}_3$  and  $\text{Fe}_3\text{C}$  on the steel surface [39]. The complete analysis result can be found in Appendix E. The steels underwent pre-corrosion (anodic galvanostatic) with current density 1 mA/cm<sup>2</sup> for 24 hours, in solution of 1% wt NaCl, 1 bar  $\text{CO}_2$ , and 20°C. Higher applied anodic current in the absence of pH stabilization chemical such as  $\text{NaHCO}_3$ , might also resulted on formation of  $\text{FeCO}_3$ , showing that supersaturation in the vicinity of steel surface could be attained in spite of low saturation in bulk solution.

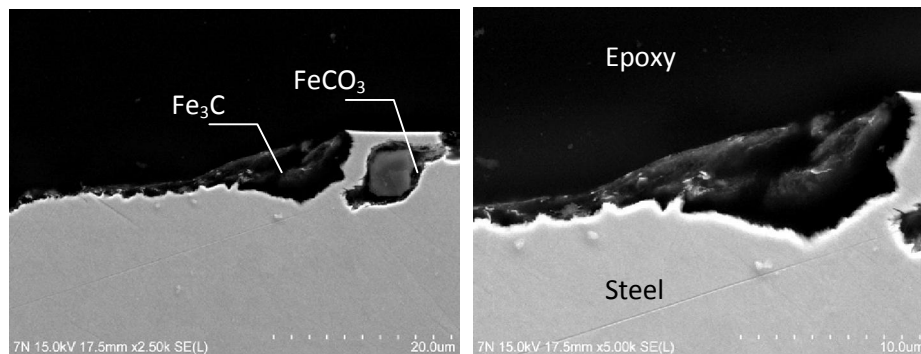


**Figure 18.** SEM images of the X-65 electrodes applied with the anodic current density of  $1 \text{ mA/cm}^2$  for 24 hours. Laethaisong [39]

#### 4.6 Future Works and Recommendation

This study has found some interesting facts on behavior of steel St-52 in solution  $0 \text{ mmol/kg HCO}_3^-$  without MEG at  $20^\circ\text{C}$  and  $40^\circ\text{C}$  which had relatively low corrosion current despite of low  $\text{FeCO}_3$  supersaturation. This can be further investigated to find the clear reason and related it to other parameter such as steel metallurgy. It was also beneficial to expand the experiment to a higher temperature where kinetics of corrosion and  $\text{FeCO}_3$  formation are enhanced, to see the effect on the corrosion behavior of steel. Some authors proposed that protective  $\text{FeCO}_3$  formation was only formed at higher temperature, above  $60^\circ\text{C}$ , and below this temperature, an open porous film was formed [36]. Thus, it can be observed whether there is any difference in the mechanism, corrosion behavior, and corrosion damage type. In addition, it is important to perform regular calibration on Gamry potentiostat to avoid producing inaccurate result. And, if it possible, it is better to perform several runs simultaneously for one series by using multiplexer. This can be done to improve the measurement result quantities and can detect abnormalities earlier.

## 5. CONCLUSION

CO<sub>2</sub> corrosion on pre-corroded X-65 and St-52 steel in 1% wt NaCl, 0-50% MEG, and 0-100 mmol/kg HCO<sub>3</sub><sup>-</sup> concentration was characterized by potential, Rp/Ec trend, potentiodynamic polarization, and iron concentration measurement. From the experiment result, it can be concluded that:

- The pre-corrosion step by application of anodic current modified the steel surface. Corrosion film formed on the steel surface was affected by solution composition. During anodic galvanostatic, MEG addition caused an increase in potential, and higher pH due to HCO<sub>3</sub><sup>-</sup> addition resulted in the more negative potential. Meanwhile, temperature affected the movement of potential with time. In high temperature, potential increase with time as corrosion rate was accelerated, and corrosion film formation dominated over the film dissolution.
- HCO<sub>3</sub><sup>-</sup> addition was the main cause of solution pH increment. Higher pH also increased supersaturation of FeCO<sub>3</sub>, that when combined with higher temperature will result in iron carbonate film formation.
- The increase in MEG concentration reduced corrosion current in all experiment conditions and both steels, since it modified the solution properties and retarded transport process.
- Increasing temperature from 20°C to 40°C increased the corrosion rate, except for conditions with high FeCO<sub>3</sub> supersaturation, which is found in solution of 100 mmol/kg HCO<sub>3</sub><sup>-</sup> and 50% MEG. The corrosion rate could be as low as 0.029 mA/cm<sup>2</sup> (0.34 mm/y) for X-65 and 0.02 mA/cm<sup>2</sup> (0.24 mm/y) for St-52. Meanwhile in other experiment with low or no FeCO<sub>3</sub> formation, it was higher than 1 mm/y. In other experiment conditions where iron carbonate formation is low, corrosion rate of St-52 is higher than X-65. The steel composition of St-52, which has higher carbon content, might result in higher carbide formation leading to galvanic effect and enhanced corrosion. In contrary, at higher FeCO<sub>3</sub> supersaturation, the positive effect of iron carbide

was to provide anchoring site for formation of protective iron carbonate that could lower corrosion rate.

- Analysis of potentiodynamic curve after pre-corrosion step showed that addition of MEG and  $\text{HCO}_3^-$  in electrolyte had no marked effect on anodic curve. On the other hand the increase in MEG and  $\text{HCO}_3^-$  reduced the limiting current and affected the shape of cathodic curve.
- Visible corrosion damage in all steel was uniform corrosion, except for experiment with protective  $\text{FeCO}_3$  formation that had pitting corrosion.

## 6. REFERENCES

1. M. Nordsveen, S.N.R. Nyborg, and A. Stangeland, *A Mechanistic Model for Carbon Dioxide Corrosion of Mild Steel in the Presence of Protective Iron Carbonate Films Part 1: Theory and Verification*. Corrosion, 2003. **59**(05).
2. J.G. Llongueras, et al., *Mechanism of FeCO<sub>3</sub> Formation on API X70 Pipeline Steel in Brine Solutions Containing CO<sub>2</sub>*, in *CORROSION 2005*. 2005, NACE International: Houston, Tx.
3. S. Nestic, J. Postlethwaite, and S. Olsen, *An Electrochemical Model for Prediction of Corrosion of Mild Steel in Aqueous Carbon Dioxide Solutions*. Corrosion, 1996. **52**(04).
4. A. Dugstad, *Fundamental Aspects of CO<sub>2</sub> Metal Loss Corrosion - Part 1: Mechanism*, in *CORROSION 2006*. 2006, NACE International: San Diego Ca.
5. S. Nestic, et al., *Electrochemical Properties of Iron Dissolution in the Presence of CO<sub>2</sub> - Basics Revisited*, in *CORROSION 96*. 1996, NACE International: Denver, Co.
6. S. Nestic, *Key Issues Related to Modelling of Internal Corrosion of Oil and Gas Pipelines - A Review*. Corrosion Science, 2007. **49**(12): p. 4308-4338.
7. J.O.M. Bockris, D. Drazic, and A.R. Despic, *The Electrode Kinetics of The Deposition and Dissolution of Iron*. Electrochimica Acta, 1961. **4**(2-4): p. 325-361.
8. R. Nyborg, and A. Dugstad, *Understanding and Prediction of Mesa Corrosion Attack*, in *CORROSION 2003*. 2003, NACE International: San Diego Ca.

9. M.B. Kermani, and A. Morshed, *Carbon Dioxide Corrosion in Oil and Gas Production - A Compendium*. Corrosion, 2003. **59**(08).
10. E.S. Davenport, *Fundamental Characteristics of Alloy Steel*, in *Drilling and Production Practice*. 1935, American Petroleum Institute.
11. S. Al-Hassan, et al., *Effect of Microstructure on Corrosion of Steels in Aqueous Solutions Containing Carbon Dioxide*. Corrosion, 1998. **54**(06).
12. K. Videm, et al., *Surface Effects on the Electrochemistry of Iron and Carbon Steel Electrodes in Aqueous CO<sub>2</sub> Solutions*, in *CORROSION 96*. 1996, NACE International: Denver, Co.
13. T.L. Yau, *Corrosion Issues Related to Fabrication Processes and Procedures*, in *CORROSION 2006*. 2006, NACE International: San Diego Ca.
14. G. Schmitt, and M. Horstemeier, *Fundamental Aspects of CO<sub>2</sub> Metal Loss Corrosion - Part II: Influence of Different Parameters on CO<sub>2</sub> Corrosion Mechanisms*, in *CORROSION 2006*. 2006, NACE International: San Diego Ca.
15. A. Dugstad, H. Hemmer, and M. Seiersten, *Effect of Steel Microstructure on Corrosion Rate and Protective Iron Carbonate Film Formation*. Corrosion, 2001. **57**(04).
16. M. Ueda, and H. Takabe, *Effect of Environmental Factor and Microstructure on Morphology of Corrosion Products in CO<sub>2</sub> Environments*, in *CORROSION 99*. 1999, NACE International: San Antonio, Tx.
17. B. Mishra, et al., *Development of a Predictive Model for Activation-Controlled Corrosion of Steel in Solutions Containing Carbon Dioxide*. Corrosion, 1997. **53**(11).

18. S. Netic, et al., *A Mechanistic Model for Carbon Dioxide Corrosion of Mild Steel in the Presence of Protective Iron Carbonate Films Part 2: A Numerical Experiment*. Corrosion, 2003. **59**(06).
19. E.V. Hunnik, B.F.M. Pots, and E.L.J.A. Hendriksen, *The Formation of Protective FeCO<sub>3</sub> Corrosion Product Layers in CO<sub>2</sub> Corrosion*, in *CORROSION 96*. 1996, NACE International: Denver, Co.
20. J.L. Crolet, N. Thevenot, and S. Netic, *Role of Conductive Corrosion Products in the Protectiveness of Corrosion Layers*. Corrosion, 1998. **54**(03).
21. R. Nyborg, et al., *Effect of Steel Microstructure and Composition on Inhibition of CO<sub>2</sub> Corrosion*, in *CORROSION 2000*. 2000, NACE International: Orlando, Fl.
22. S. Netic, and K.-L.J. Lee, *A Mechanistic Model for Carbon Dioxide Corrosion of Mild Steel in the Presence of Protective Iron Carbonate Films Part 3: Film Growth Model*. Corrosion, 2003. **59**(07).
23. A. Dugstad, *Mechanism of Protective Film Formation During CO<sub>2</sub> Corrosion of Carbon Steel*, in *CORROSION 98*. 1998, NACE International: San Diego Ca.
24. W. Sun, S. Netic, and R.C. Woollam, *The Effect of Temperature and Ionic Strength on Iron Carbonate (FeCO<sub>3</sub>) Solubility Limit*. Corrosion Science, 2009. **51**(6): p. 1273-1276.
25. M.B. Tomson, and M.L. Johnson, *How Ferrous Carbonate Kinetics Impacts Oilfield Corrosion*, in *SPE International Symposium on Oilfield Chemistry*. 1991: Anaheim, California.
26. D.A. López, , T. Pérez, and S.N. Simison, *The Influence of Microstructure and Chemical Composition of Carbon and Low Alloy Steels in CO<sub>2</sub>*

- Corrosion. A State-of-the-art Appraisal*. Materials & Design, 2003. **24**(8): p. 561-575.
27. B. Kermani, et al., *Development of Low Carbon Cr-Mo Steels with Exceptional Corrosion Resistance for Oilfield Applications*, in *CORROSION 2001*. 2001, NACE International: Houston, Tx.
  28. A. Dugstad, and P.-E. Dronen, *Efficient Corrosion Control of Gas Condensate Pipelines by pH - Stabilization*, in *CORROSION 99*. 1999, NACE International: San Antonio, Tx.
  29. S. Olsen, *Corrosion Control by Inhibition, Environmental Aspects, and pH Control: Part II: Corrosion Control by pH Stabilization*, in *CORROSION 2006*. 2006, NACE International: San Diego Ca.
  30. A. Dugstad, and M. Seiersten, *pH-stabilisation, a Reliable Method for Corrosion Control of Wet Gas Pipelines*, in *SPE International Symposium on Oilfield Corrosion*. 2004: Aberdeen, United Kingdom.
  31. N.G. Thompson, and J.H. Payer, *DC Electrochemical Test Methods*. 1998, Houston, Tex.: NACE International. X, 124 s.
  32. P.R. Roberge, *Corrosion Engineering: Principles and Practice*. 2008, New York: McGraw-Hill. XIV, 754 s.
  33. E. Gulbrandsen, and J.H. Morard, *Why Does Glycol Inhibit CO<sub>2</sub> Corrosion?*, in *CORROSION 98*. 1998, NACE International: San Diego Ca.
  34. J. Han, et al., *Spontaneous Passivation Observations During Scale Formation on Mild Steel in CO<sub>2</sub> Brines*. *Electrochimica Acta*. **In Press, Corrected Proof**.

35. E. Gulbrandsen, and J.H. Morard, *Study of the Possible Mechanisms of Steel Passivation in CO<sub>2</sub> Corrosion*, in *CORROSION 99*. 1999, NACE International: San Antonio, Tx.
36. J.L. Mora-Mendoza, and S. Turgoose, *Fe<sub>3</sub>C Influence on The Corrosion Rate of Mild Steel in Aqueous CO<sub>2</sub> Systems Under Turbulent Flow Conditions*. *Corrosion Science*, 2002. **44**(6): p. 1223-1246.
37. T. Berntsen, M. Seiersten, and T. Hemmingsen, *CO<sub>2</sub> Corrosion of Carbon Steel at Lower Temperatures*. *EUROCORR*, 2008.
38. J. Kvarekval, S. Skjerve, and S. Olsen, *The Effect of O<sub>2</sub> on CO<sub>2</sub> Corrosion in pH Stabilized Gas/Condensate Pipelines*, in *CORROSION 2005*. 2005, NACE International: Houston, Tx.
39. N. Laethaisong, *Carbide Formation of Carbon Steels in CO<sub>2</sub> Corrosion by Use of Applied Anodic Current*. Master Thesis, University of Stavanger, 2011.

## APPENDIX A – STEEL CERTIFICATE

### Ståldata

Stål nr:

Legering	<input type="text" value="X-65"/>	Form	<input ,="" 31,0"="" type="text" value="Rør 36" wt=""/>
Sveis	<input type="text"/>	Leverandør	<input type="text" value="Shell"/>
Prosjekt	<input type="text"/>	Lagringssted	<input type="text" value="PT-2 kjeller plass 1.7"/>
Prosjekt betegnelse	<input type="text"/>	Beholdning	<input type="text" value="Mer enn 3 kg"/>

#### Legeringselementer - grunnmateriale

C:	Si:	Mn:	S:	P:	Cr:	Ni:	V:	Mo:	Cu:	Al:	Sn:	Nb:
0.08	0.25	1.54	0.001	0.019	0.04	0.03	0.045	0.01	0.02	0.038	0.001	0.043

Mikrostruktur

En bit fra Troll-ledningen

## Ståldata

Stål nr:

Legering

Form

Sveis

Leverandør

Prosjekt

Lagingssted

Prosjekt betegnelse

Beholdning

### Legeringselementer - grunnmateriale

C:	Si:	Mn:	S:	P:	Cr:	Ni:	V:	Mo:	Cu:	Al:	Sn:	Nb:
0.13	0.38	1.29	0.008	0.015	0.07	0.09	0.035	0.01	0.34	0.05	0.015	

Mikrostruktur

## APPENDIX B - STANDARD CALIBRATION CURVE

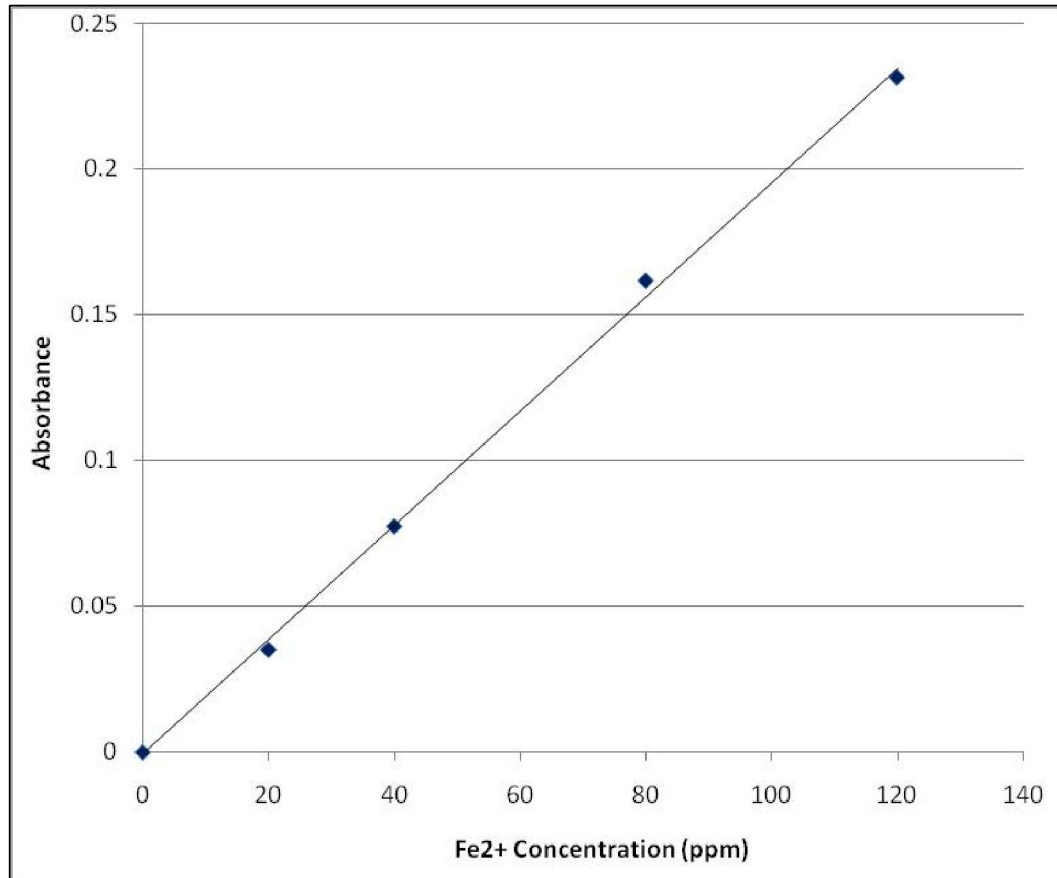


**Figure B.1** Standard calibration curve of iron concentration vs absorbance

Linear regression is shown in Equation A.1, and this equation is considered to be perfectly fitted with the datapoints since  $r^2$  value is close to 1.

$$y = 0.002 x - 0.0009 \quad (\text{A.1})$$

$$r^2 = 0.9985$$

## APPENDIX C – CATHODIC POTENTIODYNAMIC SWEEP

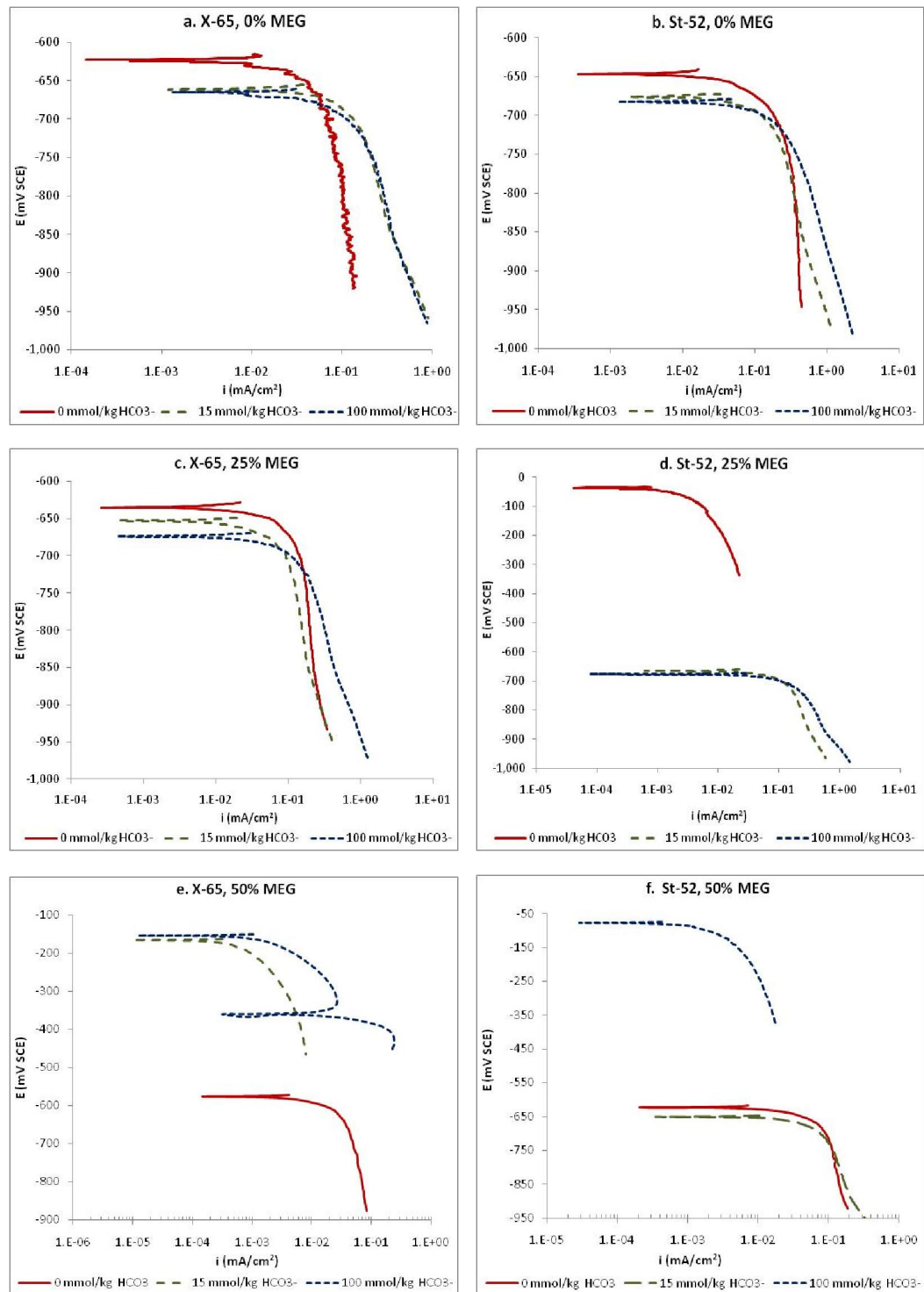


**Figure C.1** Cathodic potentiodynamic sweep prior to pre-corrosion step on series 0-100 mmol/kg HCO<sub>3</sub><sup>-</sup>, at 20°C

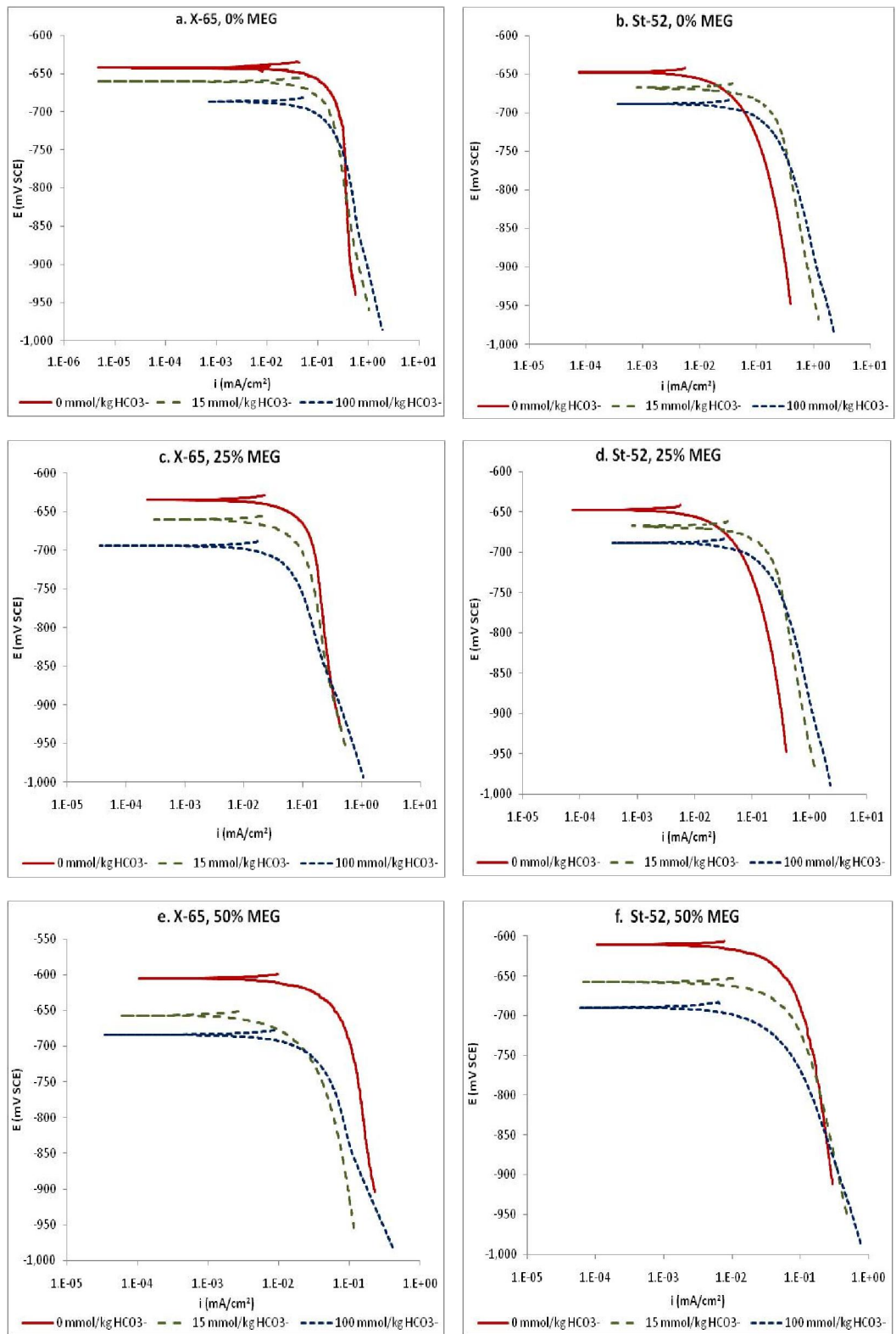


**Figure C.2** Cathodic potentiodynamic sweep after pre-corrosion step on series 0-100 mmol/kg HCO<sub>3</sub><sup>-</sup>, at 20°C

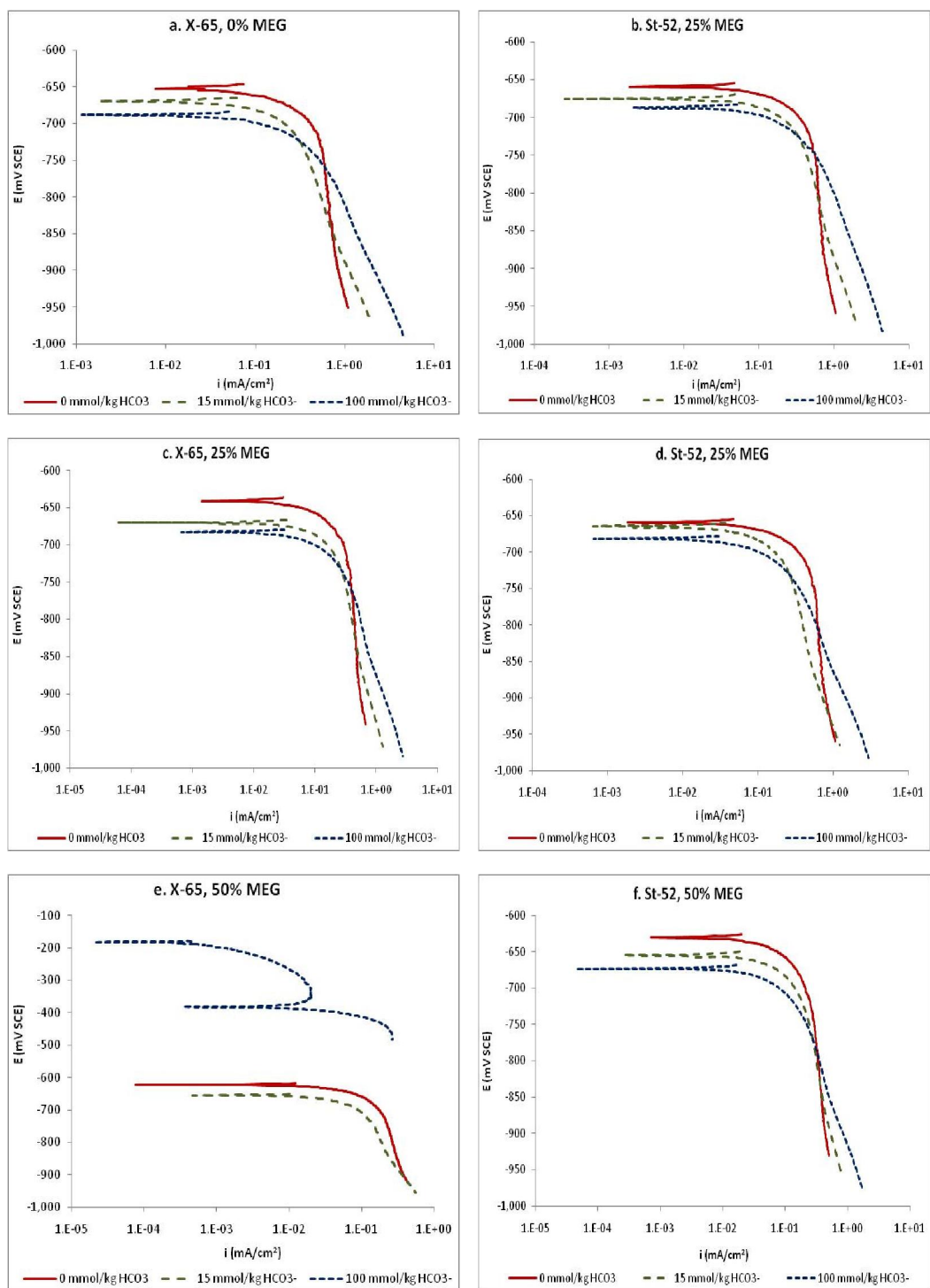


**Figure C.3** Cathodic potentiodynamic sweep prior to pre-corrosion step on series 0-100 mmol/kg HCO<sub>3</sub><sup>-</sup>, at 40°C

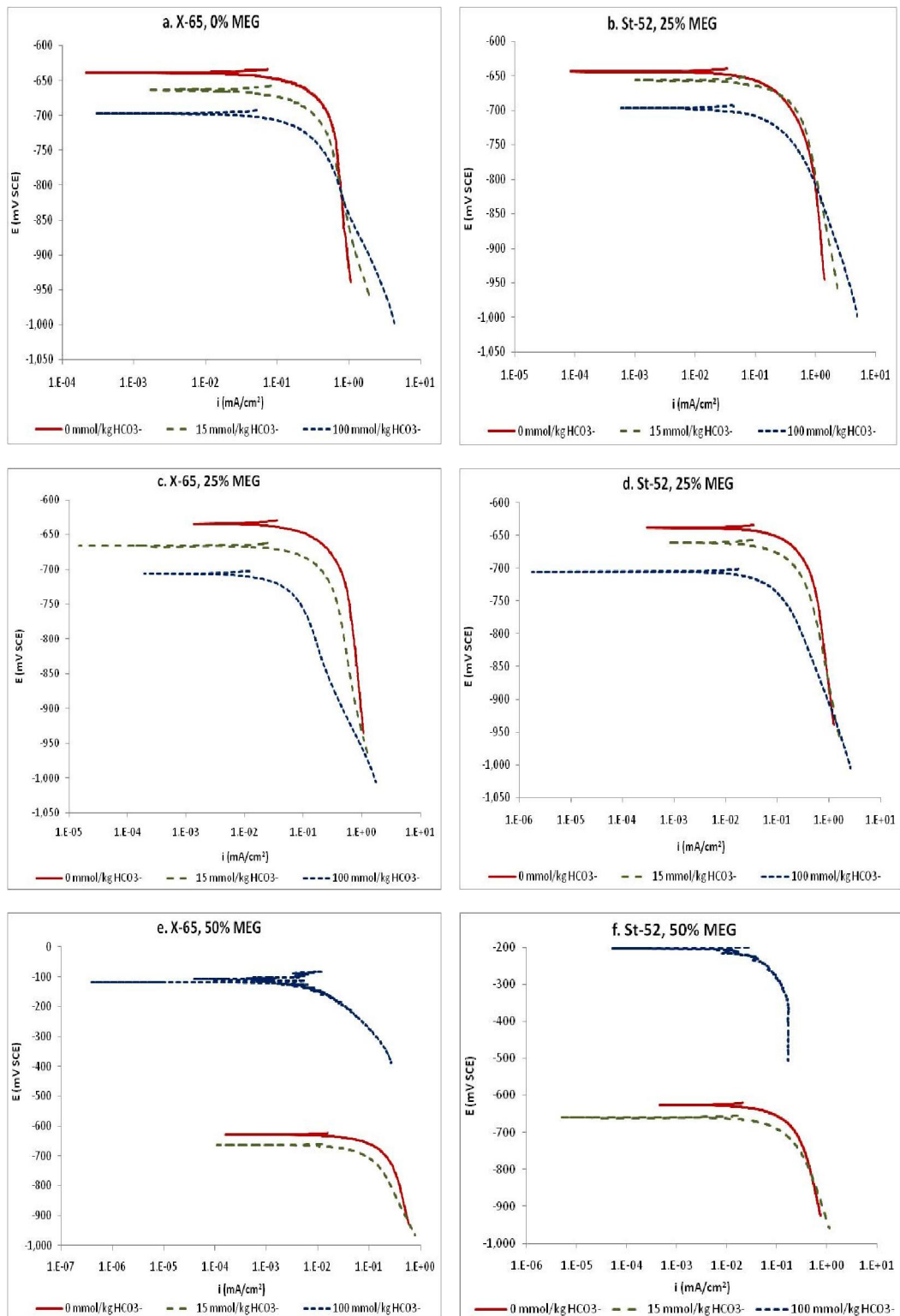


**Figure C.4** Cathodic potentiodynamic sweep after pre-corrosion step on series 0-100 mmol/kg HCO<sub>3</sub><sup>-</sup>, at 40°C

## APPENDIX D – WEIGHT LOSS

Table C.1. Weight loss measurement result

No.	T (°C)	MEG (%wt)	HCO <sub>3</sub> <sup>-</sup> (mmol/kg)	pH after purging	X-65	St-52
1	20	0	0	3.89	0.32	0.35
2			15	6.03	0.19	0.31
3			100	6.93	0.18	0.24
4		25	0	4.35	0.18	0.53
5			15	6.22	0.18	0.21
6			100	6.86	0.11	0.21
7		50	0	4.09	0.19	0.15
8			15	6.43	0.10	0.12
9			100	7.21	0.08	0.08
10	40	0	0	3.8	0.47	0.93
11			15	6.08	0.19	0.46
12			100	6.91	0.16	0.23
13		25	0	3.81	0.24	0.49
14			15	6.08	0.21	0.23
15			100	7.03	0.13	0.10
16		50	0	3.96	0.29	0.15
17			15	6.29	0.22	0.08
18			100	7.27	0.05	-0.08

## APPENDIX E - SEM IMAGES AND EDS ANALYSIS

The following SEM images and EDS analysis is a result of sample X-65, 1% wt NaCl, after being applied with anodic galvanostatic current of 1 mA/cm<sup>2</sup> for 24 hours under 1 bar CO<sub>2</sub> purging [39].

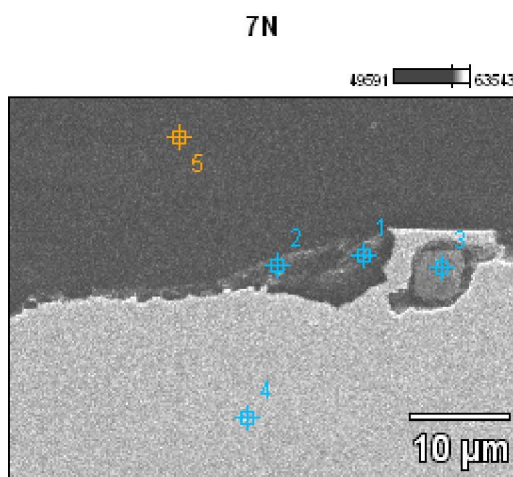


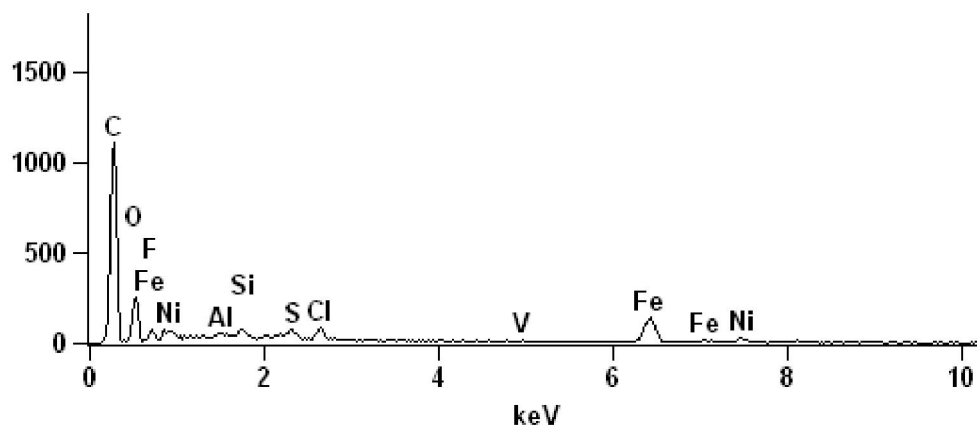
Image Name: 7N

Accelerating Voltage: 15.0 kV

Magnification: 2500

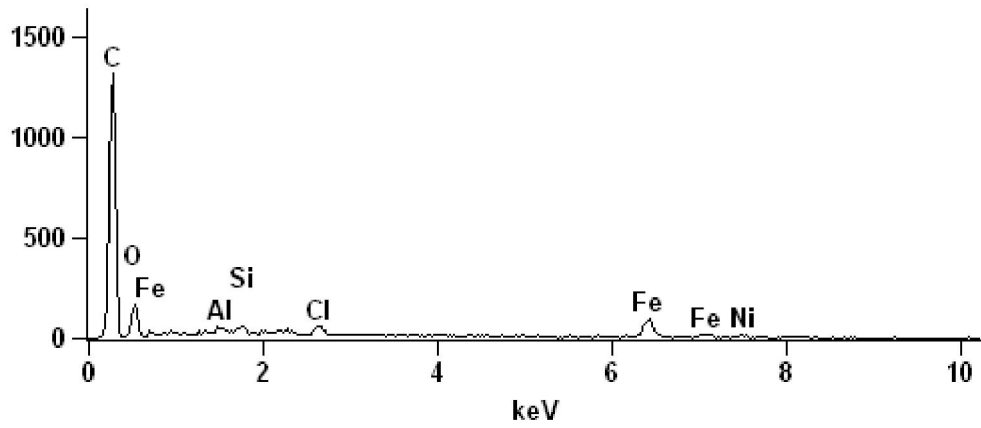
Full scale counts: 1105

7N\_pt1



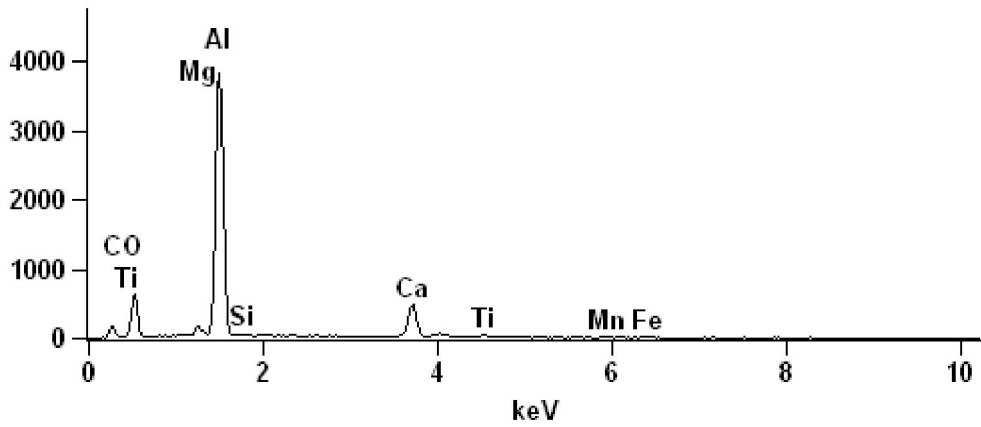
Full scale counts: 1315

7N\_pt2



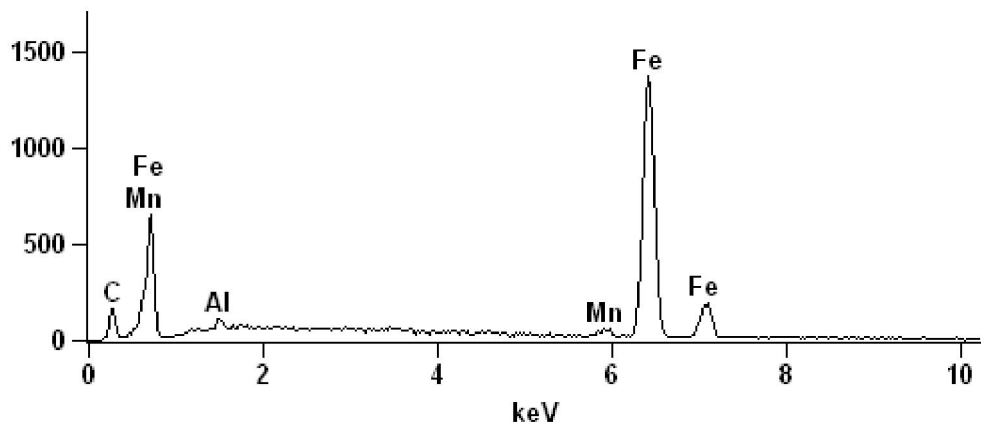
Full scale counts: 3824

7N\_pt3



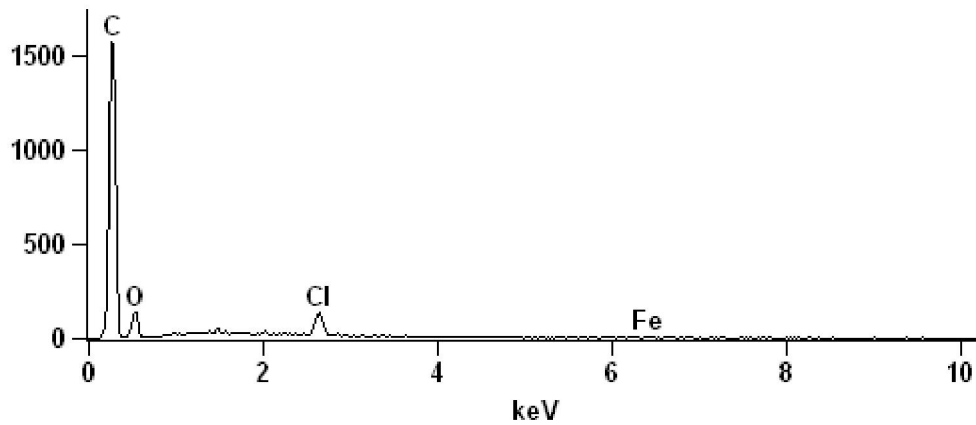
Full scale counts: 1374

7N\_pt4



Full scale counts: 1565

7N\_pt5



Weight %

	C-K	O-K	F-K	Mg-K	Al-K	Si-K	S-K	Cl-K	Ca-K	Ti-K	V-K	Mn-K	Fe-K	Ni-K
7N_pt1	59.59	23.99	0.84		0.25	0.39	0.50	0.80			0.26		10.22	3.16
7N_pt2	69.27	20.85			0.16	0.23		0.95					7.37	1.16
7N_pt3	18.07	39.40		0.91	30.87	0.35			8.18	0.74		0.27	1.20	
7N_pt4	14.12				0.82							1.55	83.52	
7N_pt5	78.22	19.08						2.01					0.69	

Atom %

	C-K	O-K	F-K	Mg-K	Al-K	Si-K	S-K	Cl-K	Ca-K	Ti-K	V-K	Mn-K	Fe-K	Ni-K
7N_pt1	72.88	22.02	0.65		0.14	0.20	0.23	0.33			0.08		2.69	0.79
7N_pt2	79.40	17.94			0.08	0.11		0.37					1.82	0.27
7N_pt3	27.82	45.54		0.69	21.16	0.23			3.78	0.29		0.09	0.40	
7N_pt4	43.06				1.11							1.03	54.80	
7N_pt5	83.77	15.34						0.73					0.16	